 CMES, vol.35, no.3, pp.181-214, 2008

A Mesh-Free DRK-Based Collocation Method for the Coupled Analysis of Functionally Graded Magneto-Electro-Elastic Shells and Plates

Chih-Ping Wu[1,2], **Kuan-Hao Chiu**[2] **and Yung-Ming Wang**[2]

Abstract: A mesh-free collocation method based on differential reproducing kernel (DRK) approximations is developed for the three-dimensional (3D) analysis of simply-supported, doubly curved functionally graded (FG) magneto-electro-elastic shells under the mechanical load, electric displacement and magnetic flux. The material properties of FG shells are firstly regarded as heterogeneous through the thickness coordinate and then specified to obey an identical power-law distribution of the volume fractions of the constituents. The novelty of the present DRK-based collocation method is that the shape functions of derivatives of reproducing kernel (RK) approximants are determined using a set of differential reproducing conditions without directly taking the differentiation towards the RK approximants. That prevents from the complicated calculations on the determination of the derivatives of RK approximants in the conventional RK methods. The present formulation is derived using the orthogonal curvilinear coordinates of doubly curved shells and can be reduced to the formulation of plates by letting the curvature radii be an infinite value. In the implementation of the present DRK-based collocation method, several crucial parameters such as the optimal support size and highest-order of the basis functions are discussed. The influence of the power-law exponent on the magnetic, electric and mechanical variables induced in the FG shells is studied.

Keyword: Mesh-free methods, Collocation methods, DRK approximants, Coupled magneto-electro-elastic effects, FG material, Static, Shells, Plates.

1 Introduction

Recently, functionally graded (FG) magneto-electro-elastic structures have been used in engineering applications for sensing, actuating and controlling purposes due to their direct and converse multi-field effects. Unlike the conventional multi-

[1] Corresponding author. Email: cpwu@mail.ncku.edu.tw
[2] Department of Civil Engineering, National Cheng Kung University, Taiwan, ROC

layered composite structures of which properties are layer-wise constants through the thickness of the structures, the through-thickness distribution of material properties for FG structures are gradually and continuously vary. That is helpful for preventing from several drawbacks such as residual stress concentration, large interlaminar stresses at interfaces between adjacent layers, etc, often occurring in multilayered structures. That type of material properties, however, also increases the complexity and difficulty for the analysis of FG structures. Since an accurate structural analysis is of much importance for the design work of those devices made up of the FG materials, the relevant subjects have considerably attracted the attention of researchers.

Some literature on three-dimensional (3D) analysis of multilayered and FG magneto-electro-elastic structures has been published. Based on the pseudo-Stroh formalism, Pan (2001), Pan and Heyliger (2003) and Pan and Han (2005) presented exact 3D solution of multilayered and FG magneto-electro-elastic plates, respectively. The material properties of the FG plates have been assumed to be exponentially distributed through the thickness coordinate. The structural behavior of simply-supported, FG plates made of piezoelectric $BaTiO_3$ and magnetostrictive $CoFe_2O_4$ materials and subjected to magneto-electro-mechanical loads has been studied. Chen and Lee (2003) proposed the alternative state space formulation to determine 3D solutions of FG magneto-electro-elastic plates using the method of propagator (or transfer) matrix. The material properties of the FG plates have been assumed to obey an identical power-law distribution of the volume fractions of the constituents. In recent papers, Wu and Tsai (2007) and Tsai and Wu (2008a, b) presented 3D solutions for the static and dynamic analyses of multilayered and FG magneto-electro-elastic shells using the method of perturbation. It has been shown that the asymptotic solutions converge rapidly and the convergent asymptotic solutions are in excellent agreement with the available 3D solutions. A comprehensive literature review on the 3D analytical approaches of the functionally graded structures made up of smart materials has been made by Wu et al. (2008a).

Several numerical methodologies have also been proposed for the approximate 3D and two-dimensional (2D) analysis of the present smart structures. Bhangale and Ganesan (2006) proposed a semi-analytical finite element method for the static analysis of FG and layered magneto-electro-elastic plates. It has been demonstrated that the FE solutions are in excellent agreement with the 3D solutions obtained by Pan and Han (2005). Heyliger and Pan (2004) and Heyliger et al. (2004) proposed a discrete-layer theory for the static behavior of multilayered magneto-electro-elastic plates. Excellent agreement has been found between this discrete-layer solutions and available 3D solutions.

In recent decades, many researchers have devoted to the development of meshless

methods such as the smooth particle hydrodynamics methods (Lucy et al., 1977), the diffuse element methods (Nayroles et al., 1992), the element-free Galerkin methods (Belytschko et al., 1994), the moving least squares method (Lancaster and Salkauskas, 1981), the meshless local Petrov-Galerkin (MLPG) method (Atluri et al.,1999; Atluri and Zhu, 1998, 2000a, b) and reproducing kernel particle methods (Liu et al., 1995). Unlike the conventional finite element methods (FEM) of which formulations and calculations of the coefficient matrix strongly rely on a grid (or mesh), the unknown approximants of previous meshless methods are entirely constructed in terms of randomly scattered nodes. It has been reported that the drawbacks of FEM in treating discontinuity, moving boundary and large deformation problems can be overcome (Chen et al., 1996; Liu et al., 1995). A comprehensive literature survey on meshless methods has been made by Belytschko et al. (1996) and Liu and Gu (2005).

Several mesh-free particle, finite point and collocation methods based on different types of approximations or interpolations have been proposed for solving the so-called strong form problems in the literature. A point collocation method based on reproducing kernel approximations has been proposed by Aluru (2000) for numerical solution of partial differential equations with appropriate boundary conditions. The point collocation method has been shown to be accurate for several one and two-dimensional problems. Oňate (1996) proposed a finite point method based on weighted least squares interpolations for the analysis of convective-diffusive transport and compressible fluid flow problems. A differential quadrature (DQ) method based on the local radial basis functions (RBF) has been proposed by Shu et al. (2003). The local RBF-based DQ method has been successfully applied to study the incompressible flows in the steady and unsteady regions (Shu et al., 2005), 2D incompressible Navier-Stokes equations (Shu et al., 2003) and 3D incompressible viscous flows with curved boundary (Shan et al., 2008).

As we aforementioned, several element-free and mesh-free methods have also been proposed for solving the so-called weak form problems based on energy principles in the literature (Atluri et al. 1998; Belytschko, et al., 1994; Liu et al., 1995). Since the computation for derivatives of those unknown approximants is complicated, Atluri et al. (2004) proposed a meshless local Petrov-Galerkin mixed finite volume method to simplify and speed up the MLPG implementation. This MLPG mixed finite volume method has been successfully applied to various elastic problems (Han and Atluri, 2004a, b; Han et al., 2005). Atluri et al. (2006a) proposed a MLPG mixed collocation method by means of using the Dirac delta function as the test function in the MLPG method. It has been concluded that the MLPG mixed collocation method is much more efficient than the MLPG finite volume method. Atluri et al. (2006b) have further proposed a MLPG mixed difference method where the

generalized finite difference method has been used for approximating the derivatives of a function using the nodal values in the local domain of definition. Various elasticity problems have been used to validate the accuracy and convergence rate of this MLPG mixed difference method.

The MLPG method has been used to study various mechanics problems of plates and shells. A MLPG method based on the moving least squares approximations has been applied for the analysis of static, dynamic and thermoelastic analyses of isotropic homogeneous plates, shells and hollow cylinders (Sladek, Sladek, Zhang and Tan, 2006; Sladek, Sladek, Wen and Aliabadi, 2006). Based on Reissner-Mindlin plate and shallow shell theories, Sladek, Sladek, Solek and Wen (2008) and Sladek, Sladek, Solek, Wen and Atluri (2008) have studied the thermal bending problems of functionally graded anisotropic plates and shallow shells, respectively, using the MLPG method.

Recently, a mesh-free differential reproducing kernel collocation method has been proposed by Wu et al. (2008b). The novelty of this method is on the modifications for the calculations of the derivatives of RK approximants. In the conventional RK methods, the shape functions of derivatives of RK approximants were obtained by directly taking the differentiation towards the shape functions of RK approximants that may result in a lengthy expression and complicated computation. In the present DRK approximations, the shape functions of derivatives of RK approximants were obtained using a set of differential reproducing conditions. A mesh-free collocation method based on the present DRK approximations was developed for the coupled analysis of FG magneto-electro-elastic shells and plates as follows.

2 Basic equations of 3D magneto-electro-elasticity

A simply-supported, doubly curved FG magneto-electro-elastic shell with heterogeneous material properties through the thickness is considered and shown in Fig. 1. A set of the orthogonal curvilinear coordinates α, β, ζ is located on the middle surface of the shell. The total thickness of the shell is $2h$. a_α and a_β denote the curvilinear dimensions in α and β directions; R_α and R_β denote the curvature radii to the middle surface of the shell, respectively.

The linear constitutive equations valid for the nature of symmetry class of magneto-electro-elastic material considered are given by

$$\sigma_i = c_{ij}\,\varepsilon_j - e_{ki}\,E_k - q_{ki}\,H_k, \tag{1}$$

$$D_l = e_{lj}\,\varepsilon_j + \eta_{lk}\,E_k + d_{lk}\,H_k, \tag{2}$$

$$B_l = q_{lj}\,\varepsilon_j + d_{lk}\,E_k + \mu_{lk}\,H_k, \tag{3}$$

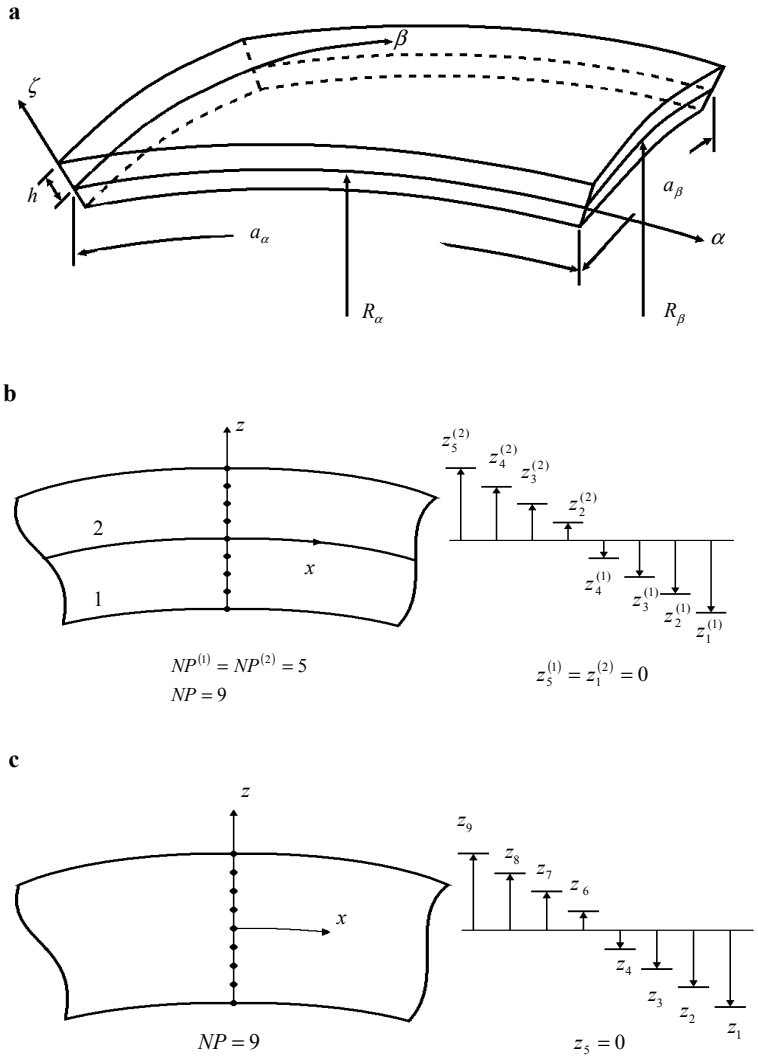

Figure 1: (a) The geometry and coordinates of a doubly curved shell; (b) The dimensionless thickness coordinates of nodal points in a two-layered shell; (c) The dimensionless thickness coordinates of nodal points in a FG shell.

where σ_i and ε_j (i, j=1-6) are the contracted notation for the stress and strain components, respectively; D_l and B_l (l=1-3) are the electric displacements and magnetic flux, respectively; E_k and H_k (k=1-3) are the electric field and magnetic field, respectively; c_{ij}, η_{lk} and μ_{lk} are the elastic, dielectric and magnetic permeability

coefficients, respectively. e_{ki}, q_{ki} and d_{lk} are the piezoelectric, piezomagnetic and magnetoelectric coefficients, respectively. The material properties are considered as heterogeneous through the thickness (i.e., $c_{ij}(\zeta)$, $\eta_{lk}(\zeta)$, $\mu_{lk}(\zeta)$, $e_{ki}(\zeta)$, $q_{ki}(\zeta)$ and $d_{lk}(\zeta)$). For an orthotropic solid, the previous material coefficients are given by

$$\mathbf{c} = \begin{bmatrix} c_{11} & c_{12} & c_{13} & 0 & 0 & 0 \\ c_{12} & c_{22} & c_{23} & 0 & 0 & 0 \\ c_{13} & c_{23} & c_{33} & 0 & 0 & 0 \\ 0 & 0 & 0 & c_{44} & 0 & 0 \\ 0 & 0 & 0 & 0 & c_{55} & 0 \\ 0 & 0 & 0 & 0 & 0 & c_{66} \end{bmatrix},$$

$$\mathbf{e} = \begin{bmatrix} 0 & 0 & e_{31} \\ 0 & 0 & e_{32} \\ 0 & 0 & e_{33} \\ 0 & e_{24} & 0 \\ e_{15} & 0 & 0 \\ 0 & 0 & 0 \end{bmatrix}, \quad \mathbf{q} = \begin{bmatrix} 0 & 0 & q_{31} \\ 0 & 0 & q_{32} \\ 0 & 0 & q_{33} \\ 0 & q_{24} & 0 \\ q_{15} & 0 & 0 \\ 0 & 0 & 0 \end{bmatrix},$$

$$\eta = \begin{bmatrix} \eta_{11} & 0 & 0 \\ 0 & \eta_{22} & 0 \\ 0 & 0 & \eta_{33} \end{bmatrix}, \quad \mathbf{d} = \begin{bmatrix} d_{11} & 0 & 0 \\ 0 & d_{22} & 0 \\ 0 & 0 & d_{33} \end{bmatrix}, \quad \mu = \begin{bmatrix} \mu_{11} & 0 & 0 \\ 0 & \mu_{22} & 0 \\ 0 & 0 & \mu_{33} \end{bmatrix}.$$

The strain-displacement relationships are

$$\begin{Bmatrix} \varepsilon_\alpha \\ \varepsilon_\beta \\ \varepsilon_\zeta \\ \gamma_{\beta\zeta} \\ \gamma_{\alpha\zeta} \\ \gamma_{\alpha\beta} \end{Bmatrix} = \begin{bmatrix} (1/\gamma_\alpha)\,\partial_\alpha & 0 & (1/\gamma_\alpha R_\alpha) \\ 0 & (1/\gamma_\beta)\,\partial_\beta & (1/\gamma_\beta R_\beta) \\ 0 & 0 & \partial_\zeta \\ 0 & \partial_\zeta - (1/\gamma_\beta R_\beta) & (1/\gamma_\beta)\,\partial_\beta \\ \partial_\zeta - (1/\gamma_\alpha R_\alpha) & 0 & (1/\gamma_\alpha)\,\partial_\alpha \\ (1/\gamma_\beta)\,\partial_\beta & (1/\gamma_\alpha)\,\partial_\alpha & 0 \end{bmatrix} \begin{Bmatrix} u_\alpha \\ u_\beta \\ u_\zeta \end{Bmatrix}, \tag{4}$$

in which $\gamma_k = 1 + \zeta/R_k$ $(k = \alpha,\ \beta)$; $\partial_i = \partial/\partial\, i$ $(i = \alpha,\ \beta,\ \zeta)$; $u_\alpha,\ u_\beta$ *and* u_ζ are the displacement components.

The stress equilibrium equations without body forces are given by

$$\gamma_\beta \sigma_{\alpha,\alpha} + \gamma_\alpha \tau_{\alpha\beta,\beta} + \gamma_\alpha\gamma_\beta \tau_{\alpha\zeta,\zeta} + \left(2/R_\alpha + 1/R_\beta + 3\zeta/R_\alpha R_\beta\right) \tau_{\alpha\zeta} = 0, \tag{5}$$

$$\gamma_\beta\, \tau_{\alpha\beta,\alpha} + \gamma_\alpha\, \sigma_{\beta,\beta} + \gamma_\alpha\gamma_\beta\, \tau_{\beta\zeta,\zeta} + \left(1/R_\alpha + 2/R_\beta + 3\zeta/R_\alpha R_\beta\right)\, \tau_{\beta\zeta} = 0, \tag{6}$$

$$\gamma_\beta\, \tau_{\alpha\zeta,\alpha} + \gamma_\alpha\, \tau_{\beta\zeta,\beta} + \gamma_\alpha\gamma_\beta\, \sigma_{\zeta,\zeta} + \left(1/R_\alpha + 1/R_\beta + 2\zeta/R_\alpha R_\beta\right)\, \sigma_\zeta - \gamma_\beta \sigma_\alpha/R_\alpha - \gamma_\alpha \sigma_\beta/R_\beta = 0. \tag{7}$$

The equations of electrostatics for the magneto-electro-elastic material without the electric charge density is

$$\gamma_\beta D_{\alpha,\alpha}+\gamma_\alpha D_{\beta,\beta}+\gamma_\alpha\gamma_\beta D_{\zeta,\zeta}+(\gamma_\beta/R_\alpha+\gamma_\alpha/R_\beta)D_\zeta=0. \tag{8}$$

The relations between the electric field and electric potential are

$$E_k=-\Phi_{,k}/\gamma_k, \tag{9}$$

where Φ denotes the electric potential; $k=\alpha,\ \beta,\ \zeta$ and $\gamma_\zeta=1$.

The equations of magnetostatics for the magneto-electro-elastic material without the magnetic charge density is

$$\gamma_\beta B_{\alpha,\alpha}+\gamma_\alpha B_{\beta,\beta}+\gamma_\alpha\gamma_\beta B_{\zeta,\zeta}+(\gamma_\beta/R_\alpha+\gamma_\alpha/R_\beta)B_\zeta=0. \tag{10}$$

The relations between the magnetic field and magnetic potential are

$$H_k=-\Psi_{,k}/\gamma_k, \tag{11}$$

where Ψ denotes the magnetic potential; $k=\alpha,\ \beta,\ \zeta$.

The boundary conditions of the problem are specified as follows:

On the lateral surfaces the transverse load $\bar{q}_\zeta^{\pm}(\alpha,\ \beta)$, electric displacement $\bar{D}_\zeta^{\pm}(\alpha,\ \beta)$ and magnetic flux $\bar{B}_\zeta^{\pm}(\alpha,\ \beta)$ are prescribed,

$$\sigma_\zeta=\bar{q}_\zeta^{\pm}(\alpha,\ \beta)\quad D_\zeta=\bar{D}_\zeta^{\pm}(\alpha,\ \beta)\text{ and }B_\zeta=\bar{B}_\zeta^{\pm}(\alpha,\ \beta)\text{ on }\zeta=\pm h. \tag{12}$$

The edge boundary conditions of the shell are considered as fully simple supports and suitably grounded where the following quantities be satisfied:

$$\sigma_\alpha=u_\beta=u_\zeta=\Phi=\Psi=0,\text{ at }\alpha=0\text{ and }\alpha=a_\alpha; \tag{13a}$$

$$\sigma_\beta=u_\alpha=u_\zeta=\Phi=\Psi=0,\text{ at }\beta=0\text{ and }\beta=a_\beta. \tag{13b}$$

There are twenty-nine basic equations in the 3D magneto-electro-elasticity as listed in Eqs. (1)-(11). Basically these equations are a system of simultaniously partial differential equations with variable coefficients. That results mathematical complexity and difficulty for an exact 3D coupled analysis of the corresponding problem. Here, an approximately 3D approach, namely the differential reproducing kernel collocation method, is used for the present analysis of doubly curved FG shells under magneto-electro-mechanical loads.

3 Nondimensionalization

In order to scale all the field variables within a close order of magnitude and prevent from the unexpected numerical instability in the computation process, we define a set of dimensionless coordinates and variables as follows:

$$x=\alpha/\sqrt{Rh},\quad y=\beta/\sqrt{Rh},\quad z=\zeta/h,\quad R_x=R_\alpha/R,\quad R_y=R_\beta/R,$$

$$u=u_\alpha/\sqrt{Rh},\quad v=u_\beta/\sqrt{Rh},\quad w=u_\zeta/R,$$

$$\sigma_x=\sigma_\alpha/Q,\quad \sigma_y=\sigma_\beta/Q,\quad \tau_{xy}=\tau_{\alpha\beta}/Q,$$

$$\tau_{xz}=\tau_{\alpha\zeta}/(Q\sqrt{h/R}),\quad \tau_{yz}=\tau_{\beta\zeta}/(Q\sqrt{h/R}),\quad \sigma_z=\sigma_\zeta R/Qh,$$

$$D_x=D_\alpha/(e\sqrt{h/R}),\quad D_y=D_\beta/(e\sqrt{h/R}),\quad D_z=D_\zeta/e,$$

$$B_x=B_\alpha/(q\sqrt{h/R}),\quad B_y=B_\beta/(q\sqrt{h/R}),\quad B_z=B_\zeta/q,$$

$$\varphi=\Phi e/Qh,\quad \psi=\Psi q/Qh, \tag{14}$$

where R, Q, e and q stand for a characteristic length, a reference elastic, piezoelectric and piezomagnetic moduli, respectively.

In the formulation the elastic displacements ($u_\alpha,\ u_\beta,\ u_\zeta$), the transverse shear and normal stresses ($\tau_{\alpha\zeta},\ \tau_{\beta\zeta},\ \sigma_\zeta$), the electric and magnetic flux (D_ζ, B_ζ) and the electric and magnetic potentials (Φ, Ψ) are selected as the primary field variables. The other field variables are the secondary field variables and can be expressed in terms of the primary variables. Introducing the set of dimensionless coordinates and variables (Eq. (14)) and using the method of direct elimination, we obtain a set of state space equations in terms of the primary field variables as follows:

$$\frac{\partial}{\partial z}\begin{bmatrix} u\\ v\\ D_z\\ B_z\\ \sigma_z\\ \tau_{xz}\\ \tau_{yz}\\ \varphi\\ \psi\\ w\end{bmatrix}=\begin{bmatrix} k_{11} & 0 & 0 & 0 & 0 & k_{16} & 0 & k_{18} & k_{19} & k_{10}\\ 0 & k_{22} & 0 & 0 & 0 & 0 & k_{27} & k_{28} & k_{29} & k_{20}\\ 0 & 0 & k_{33} & 0 & 0 & k_{18} & k_{28} & k_{38} & k_{39} & 0\\ 0 & 0 & 0 & k_{33} & 0 & k_{19} & k_{29} & k_{39} & k_{49} & 0\\ k_{51} & k_{52} & k_{53} & k_{54} & k_{55} & k_{10} & k_{20} & 0 & 0 & k_{50}\\ k_{61} & k_{62} & k_{63} & k_{64} & k_{65} & k_{66} & 0 & 0 & 0 & k_{60}\\ k_{71} & k_{72} & k_{73} & k_{74} & k_{75} & 0 & k_{77} & 0 & 0 & k_{70}\\ k_{63} & k_{73} & k_{83} & k_{84} & k_{85} & 0 & 0 & 0 & 0 & k_{80}\\ k_{64} & k_{74} & k_{84} & k_{94} & k_{95} & 0 & 0 & 0 & 0 & k_{90}\\ k_{65} & k_{75} & k_{85} & k_{95} & k_{05} & 0 & 0 & 0 & 0 & k_{00}\end{bmatrix}\begin{bmatrix} u\\ v\\ D_z\\ B_z\\ \sigma_z\\ \tau_{xz}\\ \tau_{yz}\\ \varphi\\ \psi\\ w\end{bmatrix}, \tag{15}$$

where

$$k_{11}=h/(\gamma_\alpha R R_x),\quad k_{16}=h/\tilde{c}_{55}R,\quad k_{18}=-(\tilde{e}_{15}h/\tilde{c}_{55}\gamma_\alpha R)\,\partial_x,$$

$$k_{19} = -\left(\tilde{q}_{15} h/\tilde{c}_{55}\,\gamma_\alpha R\right)\partial_x, \quad k_{10} = -\left(1/\gamma_\alpha\right)\partial_x, \quad k_{22} = h/(\gamma_\beta R R_y),$$

$$k_{27} = h/\tilde{c}_{44} R, \quad k_{28} = -\left(\tilde{e}_{24} h/\tilde{c}_{44}\,\gamma_\beta R\right)\partial_y, \quad k_{29} = -\left(\tilde{q}_{24} h/\tilde{c}_{44}\,\gamma_\beta R\right)\partial_y,$$

$$k_{20} = -\left(1/\gamma_\beta\right)\partial_y, \quad k_{33} = -\left[\left(h/\gamma_\alpha R R_x\right) + \left(h/\gamma_\beta R R_y\right)\right],$$

$$k_{38} = \left[\left(\tilde{e}_{15}^2/\tilde{c}_{55} + \tilde{\eta}_{11}\right) h/\gamma_\alpha^2 R\right]\partial_{xx} + \left[\left(\tilde{e}_{24}^2/\tilde{c}_{44} + \tilde{\eta}_{22}\right) h/\gamma_\beta^2 R\right]\partial_{yy},$$

$$k_{39} = \left[\left(\tilde{e}_{15}\tilde{q}_{15}/\tilde{c}_{55} + \tilde{d}_{11}\right) h/\gamma_\alpha^2 R\right]\partial_{xx} + \left[\left(\tilde{e}_{24}\tilde{q}_{24}/\tilde{c}_{44} + \tilde{d}_{22}\right) h/\gamma_\beta^2 R\right]\partial_{yy},$$

$$k_{49} = \left[\left(\tilde{q}_{15}^2/\tilde{c}_{55} + \tilde{\mu}_{11}\right) h/\gamma_\alpha^2 R\right]\partial_{xx} + \left[\left(\tilde{q}_{24}^2/\tilde{c}_{44} + \tilde{\mu}_{22}\right) h/\gamma_\beta^2 R\right]\partial_{yy},$$

$$k_{51} = \left[\left(\tilde{Q}_{11}/\gamma_\alpha^2 R_x\right) + \left(\tilde{Q}_{21}/\gamma_\alpha\,\gamma_\beta R_y\right)\right]\partial_x,$$

$$k_{52} = \left[\left(\tilde{Q}_{12}/\gamma_\alpha\,\gamma_\beta R_x\right) + \left(\tilde{Q}_{22}/\gamma_\beta^2 R_y\right)\right]\partial_y,$$

$$k_{53} = \left(a_{21} e/Q\,\gamma_\alpha R_x\right) + \left(a_{22} e/Q\,\gamma_\beta R_y\right),$$

$$k_{54} = \left(a_{31} q/Q\,\gamma_\alpha R_x\right) + \left(a_{32} q/Q\,\gamma_\beta R_y\right),$$

$$k_{55} = \left(a_{11} h/\gamma_\alpha R R_x\right) + \left(a_{12} h/\gamma_\beta R R_y\right) - \left(1/R_x + 1/R_y + 2hz/R R_x R_y\right)\left(h/R\,\gamma_\alpha\,\gamma_\beta\right),$$

$$k_{50} = \left(\tilde{Q}_{11}/\gamma_\alpha^2 R_x^2\right) + \left(\tilde{Q}_{12} + \tilde{Q}_{21}\right)/\gamma_\alpha\,\gamma_\beta R_x R_y + \left(\tilde{Q}_{22}/\gamma_\beta^2 R_y^2\right),$$

$$k_{61} = -\left[\left(\tilde{Q}_{11}/\gamma_\alpha^2\right)\partial_{xx} + \left(\tilde{Q}_{66}/\gamma_\beta^2\right)\partial_{yy}\right],$$

$$k_{62} = -\left[\left(\tilde{Q}_{12} + \tilde{Q}_{66}\right)/\gamma_\alpha\,\gamma_\beta\right]\partial_{xy}, \quad k_{63} = -\left(a_{21} e/Q\,\gamma_\alpha\right)\partial_x,$$

$$k_{64} = -\left(a_{31} q/Q\,\gamma_\alpha\right)\partial_x, \quad k_{65} = -\left(a_{11} h/R\,\gamma_\alpha\right)\partial_x,$$

$$k_{66} = -\left(h/R\,\gamma_\alpha\,\gamma_\beta\right)\left(2/R_x + 1/R_y + 3hz/R R_x R_y\right),$$

$$k_{60} = -\left[\left(\tilde{Q}_{11}/\gamma_\alpha^2 R_x\right) + \left(\tilde{Q}_{12}/\gamma_\alpha\,\gamma_\beta R_y\right)\right]\partial_x,$$

$$k_{71} = -\left[\left(\tilde{Q}_{21} + \tilde{Q}_{66}\right)/\gamma_\alpha\,\gamma_\beta\right]\partial_{xy}, \quad k_{72} = -\left[\left(\tilde{Q}_{66}/\gamma_\alpha^2\right)\partial_{xx} + \left(\tilde{Q}_{22}/\gamma_\beta^2\right)\partial_{yy}\right],$$

$$k_{73} = -\left(a_{22} e/Q\,\gamma_\beta\right)\partial_y, \quad k_{74} = -\left(a_{32} q/Q\,\gamma_\beta\right)\partial_y, \quad k_{75} = -\left(a_{12} h/R\,\gamma_\beta\right)\partial_y,$$

$$k_{77} = -\left(h/R\,\gamma_\alpha\,\gamma_\beta\right)\left(1/R_x + 2/R_y + 3hz/R R_x R_y\right),$$

$$k_{70} = -\left[\left(\tilde{Q}_{21}/\gamma_\alpha\,\gamma_\beta R_x\right) + \left(\tilde{Q}_{22}/\gamma_\beta^2 R_y\right)\right]\partial_y,$$

$$k_{83} = e^2 b_2/Q, \quad k_{84} = q\,e\,b_3/Q, \quad k_{85} = e\,h\,b_1/R,$$

$$k_{80} = -\left[\left(a_{21} e/Q\,\gamma_\alpha R_x\right) + \left(a_{22} e/Q\,\gamma_\beta R_y\right)\right], \quad k_{94} = q^2 c_3/Q, \quad k_{95} = q\,h\,c_1/R,$$

$$k_{90} = -\left[\left(a_{31} q/Q\,\gamma_\alpha R_x\right) + \left(a_{32} q/Q\,\gamma_\beta R_y\right)\right], \quad k_{05} = a_1 Q h^2/R^2,$$

$k_{00} = -\left[\left(a_{11}h/\gamma_\alpha RR_x\right) + \left(a_{12}h/\gamma_\beta RR_y\right)\right]$;

the relevant coefficients in the previous terms of k_{ij} are given in Appendix A.

The in-surface stresses, electric displacements and magnetic displacements are dependent field variables that can be expressed in terms of the primary variables in the following form

$$\sigma_p = \mathbf{B_1}\mathbf{u} + \mathbf{B}_2 w + \mathbf{B}_3\sigma_z + \mathbf{B}_4 D_z + \mathbf{B}_5 B_z \tag{16}$$

$$\mathbf{d} = \mathbf{B}_6\boldsymbol{\sigma}_s + \mathbf{B}_7\varphi + \mathbf{B}_8\psi, \tag{17}$$

$$\mathbf{b} = \mathbf{B}_9\boldsymbol{\sigma}_s + \mathbf{B}_8\varphi + \mathbf{B}_{10}\psi, \tag{18}$$

where

$$\boldsymbol{\sigma}_p = \begin{Bmatrix}\sigma_x\\ \sigma_y\\ \tau_{xy}\end{Bmatrix}, \quad \mathbf{u} = \begin{Bmatrix}u\\ v\end{Bmatrix}, \quad \boldsymbol{\sigma}_s = \begin{Bmatrix}\tau_{xz}\\ \tau_{yz}\end{Bmatrix}, \quad \mathbf{d} = \begin{Bmatrix}D_x\\ D_y\end{Bmatrix}, \quad \mathbf{b} = \begin{Bmatrix}B_x\\ B_y\end{Bmatrix},$$

$$\mathbf{B}_1 = \begin{bmatrix}\left(\tilde{Q}_{11}/\gamma_\alpha\right)\partial_x & \left(\tilde{Q}_{12}/\gamma_\beta\right)\partial_y\\ \left(\tilde{Q}_{21}/\gamma_\alpha\right)\partial_x & \left(\tilde{Q}_{22}/\gamma_\beta\right)\partial_y\\ \left(\tilde{Q}_{66}/\gamma_\beta\right)\partial_y & \left(\tilde{Q}_{66}/\gamma_\alpha\right)\partial_x\end{bmatrix}, \quad \mathbf{B}_2 = \begin{bmatrix}\left(\tilde{Q}_{11}/\gamma_\alpha R_x\right) + \left(\tilde{Q}_{12}/\gamma_\beta R_y\right)\\ \left(\tilde{Q}_{21}/\gamma_\alpha R_x\right) + \left(\tilde{Q}_{22}/\gamma_\beta R_y\right)\\ 0\end{bmatrix},$$

$$\mathbf{B}_3 = \begin{bmatrix}a_{11}h/R\\ a_{12}h/R\\ 0\end{bmatrix}, \quad \mathbf{B}_4 = \begin{bmatrix}a_{21}e/Q\\ a_{22}e/Q\\ 0\end{bmatrix}, \quad \mathbf{B}_5 = \begin{bmatrix}a_{31}q/Q\\ a_{32}q/Q\\ 0\end{bmatrix},$$

$$\mathbf{B}_6 = \begin{bmatrix}\left(\tilde{e}_{15}/\tilde{c}_{55}\right) & 0\\ 0 & \left(\tilde{e}_{24}/\tilde{c}_{44}\right)\end{bmatrix}, \quad \mathbf{B}_7 = \begin{bmatrix}-\left(\tilde{e}_{15}^2/\tilde{c}_{55} + \tilde{\eta}_{11}\right)\partial_x/\gamma_\alpha\\ -\left(\tilde{e}_{24}^2/\tilde{c}_{44} + \tilde{\eta}_{22}\right)\partial_y/\gamma_\beta\end{bmatrix},$$

$$\mathbf{B}_8 = \begin{bmatrix}-\left(\tilde{e}_{15}\tilde{q}_{15}/\tilde{c}_{55} + \tilde{d}_{11}\right)\partial_x/\gamma_\alpha\\ -\left(\tilde{e}_{24}\tilde{q}_{24}/\tilde{c}_{44} + \tilde{d}_{22}\right)\partial_y/\gamma_\beta\end{bmatrix}, \quad \mathbf{B}_9 = \begin{bmatrix}\left(\tilde{q}_{15}/\tilde{c}_{55}\right) & 0\\ 0 & \left(\tilde{q}_{24}/\tilde{c}_{44}\right)\end{bmatrix},$$

$$\mathbf{B}_{10} = \begin{bmatrix}-\left(\tilde{q}_{15}^2/\tilde{c}_{55} + \tilde{\mu}_{11}\right)\partial_x/\gamma_\alpha\\ -\left(\tilde{q}_{24}^2/\tilde{c}_{44} + \tilde{\mu}_{22}\right)\partial_y/\gamma_\beta\end{bmatrix}.$$

The dimensionless form of boundary conditions of the problem are specified as follows:

On the lateral surfaces, the transverse load, normal electric displacement and normal magnetic flux are prescribed,

$$\sigma_z = \bar{q}_z^{\pm}(x, y) \quad D_z = \bar{D}_z^{\pm}(x, \quad y), \quad B_z = \bar{B}_z^{\pm}(x, \quad y) \quad \text{on} \quad z = \pm 1. \tag{19}$$

where $\bar{q}_z^{\pm} = \bar{q}_\zeta^{\pm} R/Qh$, $\bar{D}_z^{\pm} = \bar{D}_\zeta^{\pm}/e$, $\bar{B}_z^{\pm} = \bar{B}_\zeta^{\pm}/q$.

At the edges, the following quantities are satisfied:

$$\sigma_x = v = w = \varphi = \psi = 0, \text{ at } x = 0 \text{ and } x = a_\alpha/\sqrt{Rh}; \tag{20a}$$

$$\sigma_y = u = w = \varphi = \psi = 0, \text{ at } y = 0 \text{ and } y = a_\beta/\sqrt{Rh}. \tag{20b}$$

4 The DRK approximations

In the present paper, a newly-proposed DRK-based collocation method (Wu et al., 2008a) was used for the coupled analysis of FG magneto-electro-elastic shells. The relevant DRK approximations were briefly interpreted as follows.

4.1 Reproducing kernel approximants

It is assumed that there are *NP* discrete points randomly selected and located at $x_1, x_2, \cdots, x_{NP}$, respectively, in the domain. The reproducing kernel approximant $u^a(x)$ of unknown function $u(x)$, $\forall\ x \in \Omega$, is defined as

$$u^a(x) = \sum_{l=1}^{NP} \phi_l(x)\, \hat{u}_l \tag{21}$$

where

$$\phi_l(x) = w_a(x-x_l)\, C(x;\, x-x_l), \quad C(x;\, x-x_l) = \mathbf{P}^T(x-x_l)\, \mathbf{b}(x),$$

$$\mathbf{P}^T(x-x_l) = \begin{bmatrix} 1 & (x-x_l) & (x-x_l)^2 & \cdots & (x-x_l)^n \end{bmatrix},$$

$$\mathbf{b}^T(x) = \begin{bmatrix} b_0(x) & b_1(x) & b_2(x) & \cdots & b_n(x) \end{bmatrix};$$

$\hat{u}_l$ ($l = 1, 2, \cdots, NP$) are the fictitious nodal values and are not the nodal values of $u^a(x)$ in general; $\phi_l(x)$ is the shape functions of $u^a(x)$ at $x = x_l$; $w_a(x-x_l)$ is the weight function centered at x_l with a support size a, $C(x;\, x-x_l)$ is the correction function; $b_j(x)$ ($j = 0, 1, 2, \cdots, n$) are the undetermined functions and will be determined by satisfying the reproducing conditions, and n is the highest order of the basis functions.

By selecting the complete n^{th}-degree polynomials as the basis functions to be reproduced, we obtain a set of reproducing conditions to determine the undetermined functions of $b_l(x)$ in Eq. (21). The reproducing conditions are given as

$$\sum_{l=1}^{NP} \phi_l(x)\, x_l^m = x^m \quad m = 0, 1, 2, \cdots, n. \tag{22}$$

The previous set of reproducing conditions can be rewritten in a matrix form of

$$\sum_{l=1}^{NP} \mathbf{P}(x-x_l)\, \phi_l(x) = \sum_{l=1}^{NP} \mathbf{P}(x-x_l)\, w_a(x-x_l)\, \mathbf{P}^T(x-x_l)\, \mathbf{b}(x) = \mathbf{P}(0), \tag{23}$$

where $\mathbf{P}(0) = \begin{bmatrix} 1 & 0 & 0 & \cdots & 0 \end{bmatrix}^T$.

According to the set of reproducing conditions, we may obtain the undetermined function matrix **b**(x) in the following form

$$\mathbf{b}(x) = \mathbf{A}^{-1}(x)\,\mathbf{P}(0), \tag{24}$$

where $\mathbf{A}(x) = \sum_{l=1}^{NP} \mathbf{P}(x-x_l)\,w_a(x-x_l)\,\mathbf{P}^T(x-x_l)$.

Substituting Eq. (24) into Eq. (21) yields the reproducing kernel shape functions in the form of

$$\phi_l(x) = w_a(x-x_l)\,\mathbf{P}^T(x-x_l)\,\mathbf{A}^{-1}(x)\,\mathbf{P}(0). \tag{25}$$

It is realized from Eq. (25) that $\phi_l(x)$ vanishes when x is not in the support of nodal point at $x = x_l$. The influence of the shape functions in the support of the referred nodal point monotonically decreases as the relative distance to the nodal point increases. The fact preserves the local character of the present scheme.

4.2 Derivatives of reproducing kernel approximants

Since the reproducing kernel approximant $u^a(x)$ is given in Eq. (21), the first-order derivative of $u^a(x)$ is therefore expressed as

$$\frac{d\,u^a(x)}{dx} = \sum_{l=1}^{NP} \phi_l^{(1)}(x)\,\hat{u}_l, \tag{26}$$

where $\phi_l^{(1)}(x)$ denote the shape functions of the first-order derivatives of $u^a(x)$.

In the present scheme, we express $\phi_l^{(1)}(x)$ in the similar form of $\phi_l(x)$ as follows:

$$\phi_l^{(1)}(x) = w_a(x-x_l)\,C_1(x;\,x-x_l), \tag{27}$$

where $C_1(x;\,x-x_l) = \mathbf{P}^T(x-x_l)\,\mathbf{b}_1(x)$,

$\mathbf{b}_1^T(x) = \left[b_0^1(x) \quad b_1^1(x) \quad b_2^1(x) \quad \cdots \quad b_n^1(x)\right]$.

The differential reproducing conditions for a set of complete n^{th}-degree polynomials are given as

$$\sum_{l=1}^{NP} \phi_l^{(1)}(x)\,x_l^m = m x^{m-1} \quad m = 0,\,1,\,2,\,\cdots,\,n. \tag{28}$$

The previous set of differential reproducing conditions can be rewritten in a matrix form of

$$\sum_{l=1}^{NP} \mathbf{P}(x-x_l)\,\phi_l^{(1)}(x) = \sum_{l=1}^{NP} \mathbf{P}(x-x_l)\,w_a(x-x_l)\,\mathbf{P}^T(x-x_l)\,\mathbf{b}_1(x) = -\mathbf{P}^{(1)}(0), \tag{29}$$

where $(-1)\left[\mathbf{P}^{(1)}(0)\right] = -\left.\frac{d\mathbf{P}(x-x_l)}{dx}\right|_{x=x_l} = \begin{bmatrix}0 & -1 & 0 & \cdots & 0\end{bmatrix}^T$.

The undetermined function matrix $\mathbf{b}_1(x)$ can then be obtained and given by

$$\mathbf{b}_1(x) = -\mathbf{A}^{-1}(x)\,\mathbf{P}^{(1)}(0), \tag{30}$$

Substituting Eq. (30) into Eq. (27) yields

$$\phi_l^{(1)}(x) = -w_a(x-x_l)\,\mathbf{P}^T(x-x_l)\,\mathbf{A}^{-1}(x)\,\mathbf{P}^{(1)}(0). \tag{31}$$

Carrying on the similar derivation to the k^{th}-order derivative of the reproducing kernel approximant leads to

$$\frac{d^k u^a(x)}{dx^k} = \sum_{l=1}^{NP} \phi_l^{(k)}(x)\,\hat{u}_l, \tag{32}$$

where

$$\phi_l^{(k)}(x) = (-1)^k w_a(x-x_l)\,\mathbf{P}^T(x-x_l)\,\mathbf{A}^{-1}(x)\,\mathbf{P}^{(k)}(0),$$

$$\mathbf{P}^{(k)}(0) = \left.\frac{d^k\mathbf{P}(x-x_l)}{dx^k}\right|_{x=x_l}.$$

It is found from observing Eqs. (21), (31) and (32) that the shape functions of reproducing kernel approximants and their derivatives are independent of one another and easy to be applied in the point collocation method.

4.3 Weight functions

In implementing the present scheme, the weight functions must be selected in advance. The conventional weight function of cubic spline is used in the present analysis and given as

$$\text{Cubic spline: } w_a(x-x_l) = w(s) = \begin{cases} 6s^3 - 6s^2 + 1 & \text{for} \quad s \le (1/2) \\ -2s^3 + 6s^2 - 6s + 2 & \text{for} \quad (1/2) < s \le 1 \\ 0 & \text{for} \quad s > 1 \end{cases}, \tag{33}$$

where $s = |x-x_l|/a$.

It is noted that a very small value of a may result in an ill-conditioned problem since the system matrix $\mathbf{A}(x)$ will become singular. On the other hand, the value of a also has to be small enough to preserve the local character of the present scheme. Hence, a compromise range of the value of a has to be studied later to ensure the accuracy and convergence of the present scheme.

5 Applications

A simply-supported, doubly curved multilayered and FG shells under magneto-electro-mechanical loads is considered in the present analysis. Three different cases of applied loads on the lateral surfaces of the magneto-electro-elastic shells are considered and given as follows:

For the cases of applied mechanical load, we consider

$$\text{Case 1. } \bar{q}_{\zeta}^{+} = q_0 \sin(\pi\alpha/a_\alpha)\sin(\pi\beta/a_\beta)\ \text{N/m}^2, \quad \bar{q}_{\zeta}^{-} = 0\ \text{N/m}^2; \quad \bar{D}_{\zeta}^{+} = 0\ \text{N/m}^2, \\ \bar{D}_{\zeta}^{-} = 0\ \text{C/m}^2; \quad \bar{B}_{\zeta}^{+} = 0\ \text{Wb/m}^2, \quad \bar{B}_{\zeta}^{-} = 0\ \text{Wb/m}^2; \text{ and } q_0 = 1\ \text{N/m}^2. \quad (34)$$

For the cases of applied electric load, we consider

$$\text{Case 2. } \bar{D}_{\zeta}^{+} = D_0 \sin(\pi\alpha/a_\alpha)\sin(\pi\beta/a_\beta)\ \text{C/m}^2, \quad \bar{D}_{\zeta}^{-} = 0\ \text{C/m}^2; \quad \bar{q}_{\zeta}^{+} = 0\ \text{N/m}^2, \\ \bar{q}_{\zeta}^{-} = 0\ \text{N/m}^2; \quad \bar{B}_{\zeta}^{+} = 0\ \text{Wb/m}^2, \quad \bar{B}_{\zeta}^{-} = 0\ \text{Wb/m}^2; \text{ and } D_0 = 1\ \text{C/m}^2. \quad (35)$$

For the cases of applied magnetic load, we consider

$$\text{Case 3. } \bar{B}_{\zeta}^{+} = B_0 \sin(\pi\alpha/a_\alpha)\sin(\pi\beta/a_\beta)\ \text{Wb/m}^2, \quad \bar{B}_{\zeta}^{-} = 0\ \text{Wb/m}^2; \quad \bar{q}_{\zeta}^{+} = 0\ \text{N/m}^2, \\ \bar{q}_{\zeta}^{-} = 0\ \text{N/m}^2; \quad \bar{D}_{\zeta}^{+} = 0\ \text{C/m}^2, \quad \bar{D}_{\zeta}^{-} = 0\ \text{C/m}^2; \quad \text{and } B_0 = 1\ \text{Wb/m}^2. \quad (36)$$

5.1 The method of double Fourier series expansion

The method of double Fourier series expansion is applied to reduce the system of partial differential equations (Eq. (15)) to a system of ordinary differential equations. By satisfying the edge boundary conditions, we express the primary variables in the following form

$$(u, \quad \tau_{xz}) = \sum_{\hat{m}=1}^{\infty}\sum_{\hat{n}=1}^{\infty} (u_{\hat{m}\hat{n}}(z), \quad \tau_{xz\hat{m}\hat{n}}(z)) \cos\tilde{m}x \sin\tilde{n}y, \quad (37)$$

$$(v, \quad \tau_{yz}) = \sum_{\hat{m}=1}^{\infty}\sum_{\hat{n}=1}^{\infty} (v_{\hat{m}\hat{n}}(z), \quad \tau_{yz\hat{m}\hat{n}}(z)) \sin\tilde{m}x \cos\tilde{n}y, \quad (38)$$

$$(w,\ \sigma_z,\ \varphi,\ \psi,\ D_z,\ B_z) = \\ \sum_{\hat{m}=1}^{\infty}\sum_{\hat{n}=1}^{\infty} (w_{\hat{m}\hat{n}}(z),\ \sigma_{z\hat{m}\hat{n}}(z),\ \varphi_{\hat{m}\hat{n}}(z),\ \psi_{\hat{m}\hat{n}}(z),\ D_{z\hat{m}\hat{n}}(z),\ B_{z\hat{m}\hat{n}}(z)) \sin\tilde{m}x \sin\tilde{n}y, \quad (39)$$

where $\tilde{m} = \hat{m}\pi\sqrt{Rh}/a_\alpha$, $\tilde{n} = \hat{n}\pi\sqrt{Rh}/a_\beta$, $\hat{m}$ and $\hat{n}$ are positive integers.

For brevity, the symbols of summation are omitted in the following derivation. Using the set of dimensionless coordinates and field variables ((Eq. (14)) and substituting the Eqs. (37)-(39) in Eq. (15), we have the resulting equations as follows:

$$\frac{d}{dz}\begin{bmatrix} u_{\hat{m}\hat{n}} \\ v_{\hat{m}\hat{n}} \\ D_{z\hat{m}\hat{n}} \\ B_{z\hat{m}\hat{n}} \\ \sigma_{z\hat{m}\hat{n}} \\ \tau_{xz\hat{m}\hat{n}} \\ \tau_{yz\hat{m}\hat{n}} \\ \varphi_{\hat{m}\hat{n}} \\ \psi_{\hat{m}\hat{n}} \\ w_{\hat{m}\hat{n}} \end{bmatrix} = \begin{bmatrix} \bar{k}_{11} & 0 & 0 & 0 & 0 & \bar{k}_{16} & 0 & \bar{k}_{18} & \bar{k}_{19} & \bar{k}_{10} \\ 0 & \bar{k}_{22} & 0 & 0 & 0 & 0 & \bar{k}_{27} & \bar{k}_{28} & \bar{k}_{29} & \bar{k}_{20} \\ 0 & 0 & \bar{k}_{33} & 0 & 0 & -\bar{k}_{18} & -\bar{k}_{28} & \bar{k}_{38} & \bar{k}_{39} & 0 \\ 0 & 0 & 0 & \bar{k}_{33} & 0 & -\bar{k}_{19} & -\bar{k}_{29} & \bar{k}_{39} & \bar{k}_{49} & 0 \\ \bar{k}_{51} & \bar{k}_{52} & \bar{k}_{53} & \bar{k}_{54} & \bar{k}_{55} & -\bar{k}_{10} & -\bar{k}_{20} & 0 & 0 & \bar{k}_{50} \\ \bar{k}_{61} & \bar{k}_{62} & \bar{k}_{63} & \bar{k}_{64} & \bar{k}_{65} & \bar{k}_{66} & 0 & 0 & 0 & \bar{k}_{60} \\ \bar{k}_{71} & \bar{k}_{72} & \bar{k}_{73} & \bar{k}_{74} & \bar{k}_{75} & 0 & \bar{k}_{77} & 0 & 0 & \bar{k}_{70} \\ -\bar{k}_{63} & -\bar{k}_{73} & \bar{k}_{83} & \bar{k}_{84} & \bar{k}_{85} & 0 & 0 & 0 & 0 & \bar{k}_{80} \\ -\bar{k}_{64} & -\bar{k}_{74} & \bar{k}_{84} & \bar{k}_{94} & \bar{k}_{95} & 0 & 0 & 0 & 0 & \bar{k}_{90} \\ -\bar{k}_{65} & -\bar{k}_{75} & \bar{k}_{85} & \bar{k}_{95} & \bar{k}_{05} & 0 & 0 & 0 & 0 & \bar{k}_{00} \end{bmatrix} \begin{bmatrix} u_{\hat{m}\hat{n}} \\ v_{\hat{m}\hat{n}} \\ D_{z\hat{m}\hat{n}} \\ B_{z\hat{m}\hat{n}} \\ \sigma_{z\hat{m}\hat{n}} \\ \tau_{xz\hat{m}\hat{n}} \\ \tau_{yz\hat{m}\hat{n}} \\ \varphi_{\hat{m}\hat{n}} \\ \psi_{\hat{m}\hat{n}} \\ w_{\hat{m}\hat{n}} \end{bmatrix}, \quad (40)$$

where $\bar{k}_{ij}$ (i, j=1-10) are given in Appendix B.

5.2 The mesh-free DRK-based collocation method

Equation (40) represents a system of ten simultaneously linear ordinary differential equations in terms of ten primary variables. A mesh-free collocation method based on the present DRK approximations is applied to determine the primary variables in the elastic, electric and magnetic fields. Once these primary variables are determined, the dependent variables can then be calculated using Eqs. (16)-(18).

5.2.1 Multilayered magneto-electro-elastic shells

The present mesh-free DRK-based collocation method is applied to the coupled analysis of multilayered magneto-electro-elastic shells. The through-thickness distributions of material properties of the shell are the layerwise Heaviside functions

and given by

$$g_{ij}(\zeta) = \sum_{m=1}^{NL} g_{ij}^{(m)} \left[H(\zeta - \zeta_m) - H(\zeta - \zeta_{m+1}) \right], \tag{41}$$

where NL denotes the total number of layers constituting the shell; $g_{ij}^{(m)}$ refer to the coefficients of c_{ij}, e_{ij}, q_{ij}, η_{ij}, d_{ij} and μ_{ij} of the m^{th}-layer in general; $H(\zeta)$ is the Heaviside function; ζ_m and ζ_{m+1} are the distances measured from the middle surface of the shell to the bottom and top surfaces of the m^{th}-layer, respectively.

Selecting $NP^{(m)}$ nodal points along the thickness coordinate from bottom to top surfaces of the m^{th}-layer and applying the present DRK approximations to Eq. (40) at each nodal point, we obtain

$$\left(\sum_{l=1}^{NP^{(m)}} \phi_l^{(1)}(z_r^{(m)}) \left(\hat{F}_i^{(m)} \right)_l \right) - \bar{k}_{ij}^{(m)} \left(\sum_{l=1}^{NP^{(m)}} \phi_l(z_r^{(m)}) \left(\hat{F}_j^{(m)} \right)_l \right) = 0, \tag{42}$$

where the subscripts $i,\ j = 1, 2, 3, \cdots, 10$ and $r = 1, 2, 3, \cdots, NP^{(m)}$; the superscript $m = 1, 2, 3, \cdots, NL$;

$$\hat{\mathbf{F}}^{(m)} = \left\{ \hat{u}^{(m)} \quad \hat{v}^{(m)} \quad \hat{D}_z^{(m)} \quad \hat{B}_z^{(m)} \quad \hat{\sigma}_z^{(m)} \quad \hat{\tau}_{xz}^{(m)} \quad \hat{\tau}_{yz}^{(m)} \quad \hat{\varphi}^{(m)} \quad \hat{\psi}^{(m)} \quad \hat{w}^{(m)} \right\}^T$$

and $\left(\hat{F}_j^{(m)} \right)_l$ denotes the fictitious nodal value of the j^{th}-primary variable in $\hat{\mathbf{F}}^{(m)}$ at the l^{th}-nodal point of the m^{th}-layer; $z_r^{(m)}$ denotes the thickness coordinate of r^{th}-referred nodal point in the m^{th}-layer.

Similarly, the DRK approximations were applied for the boundary conditions on the lateral surfaces are given by

$$\sum_{l=1}^{NP^{(1)}} \phi_l(z=-1) \left(\hat{F}_3^{(1)} \right)_l = 0, \quad \sum_{l=1}^{NP^{(1)}} \phi_l(z=-1) \left(\hat{F}_4^{(1)} \right)_l = 0,$$

$$\sum_{l=1}^{NP^{(1)}} \phi_l(z=-1) \left(\hat{F}_5^{(1)} \right)_l = 0,$$

$$\sum_{l=1}^{NP^{(1)}} \phi_l(z=-1) \left(\hat{F}_6^{(1)} \right)_l = 0, \quad \sum_{l=1}^{NP^{(1)}} \phi_l(z=-1) \left(\hat{F}_7^{(1)} \right)_l = 0; \tag{43}$$

$$\sum_{l=1}^{NP^{(NL)}} \phi_l(z=1) \left(\hat{F}_3^{(NL)} \right)_l = (\text{either } \bar{D}_0 \text{ or } 0),$$

$$\sum_{l=1}^{NP^{(NL)}} \phi_l(z=1)\left(\hat{F}_4^{(NL)}\right)_l = (\text{either } \bar{B}_0 \text{ or } 0),$$

$$\sum_{l=1}^{NP^{(NL)}} \phi_l(z=1)\left(\hat{F}_5^{(NL)}\right)_l = (\text{either } \bar{q}_0 \text{ or } 0), \quad \sum_{l=1}^{NP^{(NL)}} \phi_l(z=1)\left(\hat{F}_6^{(NL)}\right)_l = 0,$$

$$\sum_{l=1}^{NP^{(NL)}} \phi_l(z=1)\left(\hat{F}_7^{(NL)}\right)_l = 0, \tag{44}$$

where $\bar{D}_0 = D_0/e$, $\bar{B}_0 = B_0/q$ and $\bar{q}_0 = q_0 R/Qh$.

The DRK approximants were also applied for the continuity conditions at interfaces between adjacent layers and given by

$$\sum_{l=1}^{NP^{(m)}} \phi_l(z=z_{NP}^{(m)})\left(\hat{F}_i^{(m)}\right)_l = \sum_{l=1}^{NP^{(m+1)}} \phi_l(z=z_1^{(m+1)})\left(\hat{F}_i^{(m+1)}\right)_l$$
$$\text{for } i=1,2,3,\cdots,10 \text{ and } m=1,2,\cdots,(NL-1). \tag{45}$$

Equations (42)-(45) represent a linear mathematical system consisting of $[(10\times NP^{(m)}\times NL)+(10\times NL)]$ simultaneously algebraic equations in terms of $(10\times NP^{(m)}\times NL)$ unknowns. The weighted least squares method is used in the present analysis where the weight number for both the lateral boundary conditions and continuity conditions is taken to be 10000 and for state space equations is 1.

5.2.2 *FG magneto-electro-elastic shells*

In the present paper, the material properties of the FG shells are assumed to obey the identical power-law distribution of the volume fractions of the constituents and are given by

$$g_{ij}(\zeta) = g_{ij}^{(t)}\,\Gamma(\zeta) + g_{ij}^{(b)}\,[1-\Gamma(\zeta)], \tag{46}$$

where the superscripts t and b in the parentheses denote the top and bottom surfaces of the shell, respectively. $\Gamma(\zeta)$ denotes the volume fraction and is defined as $\Gamma(\zeta) = \left(\frac{\zeta+h}{2h}\right)^{\kappa}$. κ is the power-law exponent which represents the degree of the material gradient along the thickness. As $\kappa = 0$ and $\kappa = \infty$, the present FG magneto-electro-elastic shell reduces to a homogeneous magneto-electro-elastic shell with material properties $g_{ij}^{(t)}$ and $g_{ij}^{(b)}$, respectively. As $\kappa = 1$, it represents that the material properties of the FG shell linearly varied through the thickness coordinate.

The present DRK-based collocation method is applied to the coupled analysis of a FG doubly curved shell. Selecting *NP* nodal points along the thickness coordinate from bottom to top surfaces of the shell with a uniform spacing and applying the present DRK approximations to Eq. (40) at each nodal point, we obtain

$$\left(\sum_{l=1}^{NP} \phi_l^{(1)}(z_r)\left(\hat{F}_i\right)_l\right) - \bar{k}_{ij}\left(\sum_{l=1}^{NP} \phi_l(z_r)\left(\hat{F}_j\right)_l\right) = 0$$
$$\text{for } i = 1, 2, 3, \cdots, 10 \text{ and } r = 1, 2, 3, \cdots, NP, \quad (47)$$

where $\hat{\mathbf{F}} = \left\{\hat{u} \quad \hat{v} \quad \hat{D}_z \quad \hat{B}_z \quad \hat{\sigma}_z \quad \hat{\sigma}_{xz} \quad \hat{\sigma}_{yz} \quad \hat{\varphi} \quad \hat{\psi} \quad \hat{w}\right\}^T$ and $\left(\hat{F}_j\right)_l$ denotes the fictitious nodal value of j^{th}-primary variable in $\hat{\mathbf{F}}$ at the l^{th}-nodal point; z_r denotes the thickness coordinate of r^{th} -referred nodal point.

Similarly, the DRK approximations were applied for the boundary conditions on the lateral surfaces of the shell are given by

$$\sum_{l=1}^{NP} \phi_l(z=-1)\left(\hat{F}_3\right)_l = 0, \quad \sum_{l=1}^{NP} \phi_l(z=-1)\left(\hat{F}_4\right)_l = 0, \quad \sum_{l=1}^{NP} \phi_l(z=-1)\left(\hat{F}_5\right)_l = 0,$$
$$\sum_{l=1}^{NP} \phi_l(z=-1)\left(\hat{F}_6\right)_l = 0, \quad \sum_{l=1}^{NP} \phi_l(z=-1)\left(\hat{F}_7\right)_l = 0; \quad (48)$$

$$\sum_{l=1}^{NP} \phi_l(z=1)\left(\hat{F}_3\right)_l = (\text{either } \bar{D}_0 \text{ or } 0), \quad \sum_{l=1}^{NP} \phi_l(z=1)\left(\hat{F}_4\right)_l = (\text{either } \bar{B}_0 \text{ or } 0),$$
$$\sum_{l=1}^{NP} \phi_l(z=1)\left(\hat{F}_5\right)_l = (\text{either } \bar{q}_0 \text{ or } 0), \quad \sum_{l=1}^{NP} \phi_l(z=1)\left(\hat{F}_6\right)_l = 0,$$
$$\sum_{l=1}^{NP} \phi_l(z=1)\left(\hat{F}_7\right)_l = 0. \quad (49)$$

Equations (47)-(49) represent a linear mathematical system consisting of $[(10 \times NP) + 10]$ simultaneously algebraic equations in terms of (10x*NP*) unknowns. A weighted least squares method is used in the present analysis where the weight number for the lateral boundary conditions is taken to be 10000 and for state space equations is 1.

6 Illustrative examples

6.1 Multilayered magneto-electro-elastic plates

Exact solution of the [B/F] and [F/B/F] layered magneto-electro-elastic plates under mechanical loads has been presented by Pan and Heyliger (2003) using the

method of propagator matrix where the character B in square bracket stands for a piezoelectric layer of $BaTiO_3$ material and the character F stands for a magnetostrictive layer of $CoFe_2O_4$ material. The previous problem was also analyzed by Heyliger et al. (2004) using a discrete-layer theory and by Wu and Tsai (2007) using the method of perturbation. The present formulation of DRK-based collocation scheme for shells can be reduced to the one for plates by letting $1/R_\alpha = 1/R_\beta = 0$.

In the cases of [B/F] layered plates, the layer of $BaTiO_3$ is on the top and that of $CoFe_2O_4$ is on the bottom of the two-layered plate. Each layer of the plate is of equal thickness. The elastic, piezoelectric, dielectric and magnetic properties of $CoFe_2O_4$ and $BaTiO_3$ materials are given in Table 1. The geometric parameters are given as $a_\alpha = 0.01$ m, $2h = 0.001$ m such that the span-to-thickness ratio $S = a_\alpha/2h = 10$. The loading condition on the lateral surface of the plate is considered as $\bar{q}_\zeta^+ = q_0 \sin(\pi\alpha/a_\alpha)$ and $\bar{q}_\zeta^- = 0$ where $q_0 = 1$ N/m^2.

Table 2 shows the present DRK collocation solutions of elastic, electric and magnetic field variables at the interface of the [B/F] layered plate. In the present analysis, a uniform spacing (Δx_3) for each pair of neighboring nodal points is used where $\Delta x_3 = 2h^{(m)}/(NP^{(m)} - 1)$ and $m = 1, 2$; $NP = \sum_{m=1}^{NL} NP^{(m)} - (NL - 1)$; $2h^{(m)}$ denotes the thickness of the m^{th}-layer and $2h^{(m)} = z_{NP}^{(m)} - z_1^{(m)}$. The effects of the highest order of basis functions (n) and the support size (a) on the present solutions are presented where the values of (n, a) are taken to be (2, $2.1\Delta x_3$), (2, $3.1\Delta x_3$) and (3, $3.1\Delta x_3$). The total number of nodal points is taken as NP=7, 9, 11, 21 (i.e., $NP^{(m)}$=4, 5, 6, 11, respectively, and m=1, 2). The accuracy and rate of convergence of the present method are validated by comparing the present solutions with the available exact 3D solutions (Pan and Heyliger, 2003; Wu and Tsai, 2007) and approximate 3D solutions (Heyliger et al., 2004). It is shown from Table 2 that the present solutions with n=3 and a=$3.1\Delta x_3$ yield more accurate results than the others and their 11-nodes solutions are in excellent agreement with the available 3D solutions.

Table 3 considers a simply-supported, [F/B/F] layered plate under the mechanical load (i.e., $\bar{q}_\zeta^+ = q_0 \sin(\pi\alpha/a_\alpha) \sin(\pi\beta/a_\beta)$, $\bar{q}_\zeta^- = 0$ and $q_0 = 1$ N/m^2). The geometric parameters are given as $a_\alpha = a_\beta = 1$ m, $2h = 0.3$ m and $S = a_\alpha/2h = 10/3$. The total number of nodal points is taken as NP=10, 13, 16, 31 (i.e., $NP^{(m)}$ = 4, 5, 6, 11, respectively, and m=1, 2, 3). The present DRK collocation solutions at the lateral surfaces ($\zeta = \pm 0.15$m) and at the interfaces between adjecent layers ($\zeta = \pm 0.05$m) are presented where n=3, a=$3.1\Delta x_3$. Again, it is shown that the present solutions converge fast and the present convergent solutions are in excellent agreement with the available exact 3D solutions (Pan and Heyliger, 2003) and approximate 3D solutions (Heyliger and Pan, 2004).

Table 1: Elastic, piezoelectric, piezomagnetic, dielectric and magnetic properties of piezoelectric and magnetostrictive materials

Moduli	$BaTiO_3$ (Heyliger et al., 2004)	$CoFe_2O_4$ (Heyliger et al., 2004)
c_{11} (Gpa)	166.0	286.0
c_{22}	166.0	286.0
c_{33}	162.0	269.5
c_{12}	77.0	173.0
c_{13}	78.0	170.5
c_{23}	78.0	170.5
c_{44}	43.0	45.3
c_{55}	43.0	45.3
c_{66}	44.5	56.5
e_{31} $\left(\mathrm{C/m^2}\right)$	-4.4	0.0
e_{32}	-4.4	0.0
e_{33}	18.6	0.0
e_{24}	11.6	0.0
e_{15}	11.6	0.0
q_{31} (N/Am)	0.0	580.3
q_{32}	0.0	580.3
q_{33}	0.0	699.7
q_{24}	0.0	550.0
q_{15}	0.0	550.0
η_{11} $\left(\mathrm{C^2/Nm^2}\right)$	11.2e-09	0.080e-09
η_{22}	11.2e-09	0.080e-09
η_{33}	12.6e-09	0.093e-09
μ_{11} $\left(\mathrm{Ns^2/C^2}\right)$	5.0e-06	-590.0e-06
μ_{22}	5.0e-06	-590.0e-06
μ_{33}	10.0e-06	157.0e-06

6.2 Multilayered magneto-electro-elastic shells

The direct piezoelectric and piezomagnetic effects of doubly curved [F/B] and [F/B/F] layered magneto-electro-elastic shells under the mechanical load (Case 1) are studied in Figs. 2-3, respectively. The geometric parameters of the shell are S=$a_\alpha/2h$=5, $a_\alpha/a_\beta = 1$, R_α/R_β=1, R_α/a_α=5. The dimensionless variables are denoted as

$$\bar{u}_i = u_i c^*/q_0\,(2h), \quad \bar{\tau}_{ij} = \tau_{ij}/q_0, \quad \bar{\Phi} = \Phi\, e^*/q_0\,(2h), \quad \bar{D}_i = D_i\, c^*/q_0\, e^*,$$

Table 2: Mechanical, electric and magnetic field variables at the interface of the [B/F] laminated plate under mechanical load ($S = 10$)

n	a	Theories	$u_\alpha\left(0,\frac{a_\beta}{2},0\right)$	$u_\zeta\left(\frac{a_\alpha}{2},\frac{a_\beta}{2},0\right)$	$\sigma_\zeta\left(\frac{a_\alpha}{2},\frac{a_\beta}{2},0\right)$	$\Phi\left(\frac{a_\alpha}{2},\frac{a_\beta}{2},0\right)$	$\Psi\left(\frac{a_\alpha}{2},\frac{a_\beta}{2},0\right)$
2	$2.1\Delta x_3$	DRKP $NP = 7$	-0.0643e-12	7.9129e-12	0.51524	2.1615e-4	-2.4255e-7
		9	-0.0643e-12	7.9129e-12	0.51524	2.1615e-4	-2.4255e-7
		11	-0.0645e-12	7.9291e-12	0.51520	2.1486e-4	-2.3919e-7
		21	-0.0653e-12	8.0049e-12	0.51478	2.1595e-4	-2.3987e-7
2	$3.1\Delta x_3$	DRKP $NP = 7$	-0.0616e-12	7.6259e-12	0.51687	2.1055e-4	-2.3670e-7
		9	-0.0627e-12	7.7441e-12	0.51618	2.1305e-4	-2.3912e-7
		11	-0.0635e-12	7.8204e-12	0.51579	2.1337e-4	-2.3831e-7
		21	-0.0649e-12	7.9702e-12	0.51497	2.1544e-4	-2.3953e-7
3	$3.1\Delta x_3$	DRKP $NP = 7$	-0.0655e-12	8.0361e-12	0.51462	2.1631e-4	-2.4005e-7
		9	-0.0655e-12	8.0378e-12	0.51460	2.1638e-4	-2.4008e-7
		11	-0.0655e-12	8.0377e-12	0.51460	2.1637e-4	-2.4008e-7
		21	-0.0655e-12	8.0377e-12	0.51460	2.1637e-4	-2.4008e-7
		Discrete-layer sol.(Heyliger et al., 2004)	-0.0655e-12	8.0344e-12	NA	2.1637e-4	-2.4018e-7
		Exact sol. (Pan and Heyliger, 2003)	-0.0655e-12	8.0377e-12	NA	2.1637e-4	-2.4008e-7
		Exact sol. (Wu and Tsai, 2007)	-0.0655e-12	8.0377e-12	0.51460	2.1637e-4	-2.4008e-7

Table 3: Mechanical, electric and magnetic field variables at crucial positions in the [F/B/F] laminated plate under mechanical load (S=10/3)

ζ (m)	Theories	$u_\alpha\left(0,\frac{a_\beta}{2},\zeta\right)$	$u_\zeta\left(\frac{a_\alpha}{2},\frac{a_\beta}{2},\zeta\right)$	$\sigma_\zeta\left(\frac{a_\alpha}{2},\frac{a_\beta}{2},\zeta\right)$	$\Phi\left(\frac{a_\alpha}{2},\frac{a_\beta}{2},\zeta\right)$	$\Psi\left(\frac{a_\alpha}{2},\frac{a_\beta}{2},\zeta\right)$
	DRKP NP = 10	-0.27371e-11	0.97088e-11	1.00000	0.43139e-2	-0.17564e-5
	13	-0.27393e-11	0.97142e-11	1.00000	0.43157e-2	-0.17304e-5
	16	-0.27391e-11	0.97139e-11	1.00000	0.43148e-2	-0.17304e-5
0.15	31	-0.27392e-11	0.97140e-11	1.00000	0.43147e-2	-0.17302e-5
	Discrete layer sol.	-0.27194e-11	0.96774e-11	NA	0.43079e-2	-0.17381e-5
	(Heyliger and Pan, 2004)					
	Exact sol.	-0.27392e-11	0.97140e-11	NA	0.43147e-2	-0.17302e-5
	(Pan and Heyliger, 2003)					
	DRKP NP = 10	-0.05772e-11	0.99878e-11	0.73155	0.46854e-2	-0.38303e-5
	13	-0.05777e-11	0.99943e-11	0.73167	0.46835e-2	-0.38483e-5
	16	-0.05777e-11	0.99939e-11	0.73166	0.46863e-2	-0.38469e-5
	31	-0.05777e-11	0.99941e-11	0.73166	0.46863e-2	-0.38477e-5
0.05	Discrete layer sol.	-0.05730e-11	0.99571e-11	NA	0.46792e-2	-0.38689e-5
	(Heyliger and Pan, 2004)					
	Exact sol.	-0.05777e-11	0.99940e-11	NA	0.46863e-2	-0.38477e-5
	(Pan and Heyliger, 2003)					
	DRKP NP = 10	0.11408e-11	0.96575e-11	0.25863	0.41374e-2	-0.29211e-5
	13	0.11414e-11	0.96640e-11	0.25854	0.41441e-2	-0.29142e-5
	16	0.11414e-11	0.96636e-11	0.25855	0.41429e-2	-0.29137e-5
-0.05	31	0.11414e-11	0.96638e-11	0.25854	0.41431e-2	-0.29138e-5
	Discrete layer sol.	0.11374e-11	0.96269e-11	NA	0.41360e-2	-0.29314e-5
	(Heyliger and Pan, 2004)					
	Exact sol.	0.11414e-11	0.96638e-11	NA	0.41431e-2	-0.29138e-5
	(Pan and Heyliger, 2003)					
	DRKP NP = 10	0.31419e-11	0.88122e-11	0.00000	0.38094e-2	-0.21751e-5
	13	0.31441e-11	0.88178e-11	0.00000	0.38156e-2	-0.21671e-5
	16	0.31440e-11	0.88175e-11	0.00000	0.38145e-2	-0.21667e-5
-0.15	31	0.31440e-11	0.88176e-11	0.00000	0.38146e-2	-0.21670e-5
	Discrete layer sol.	0.31256e-11	0.87814e-11	NA	0.38077e-2	-0.21730e-5
	(Heyliger and Pan, 2004)					
	Exact sol.	0.31440e-11	0.88176e-11	NA	0.38146e-2	-0.21670e-5
	(Pan and Heyliger, 2003)					

$$\bar{\Psi} = \Psi q^* / q_0 (2h); \quad \bar{B}_i = B_i c^* / q_0 q^*; \tag{50}$$

where $c^* = 10 \times 10^9$ N/m^2, $e^* = 10$ C/m^2, $q^* = 10$ N/Am.

Figure 2 shows the through-thickness distributions of various variables of mechanical, electric and magnetic fields of the [F/B] layered shell where NP= 7 and 9 (i.e., $NP^{(m)} = 4$ and 5; m=1, 2). It is shown that the present DRK collocation solutions convergent rapidly and the present 9-nodes solutions are in excellent agreement with the available exact 3D solutions (Wu and Tsai, 2007). In the applied mechanical load case, the variations of electric field variables through the thickness direction in the piezoelectric layer (B) are more remarkable than those in the piezomagnostrictive layer (F). Similarly, the variations of magnetic field variables through the thickness direction in the piezomagnostrictive layer are more remarkable than those in the piezoelectric layer. In the present thick shell case (S=5),

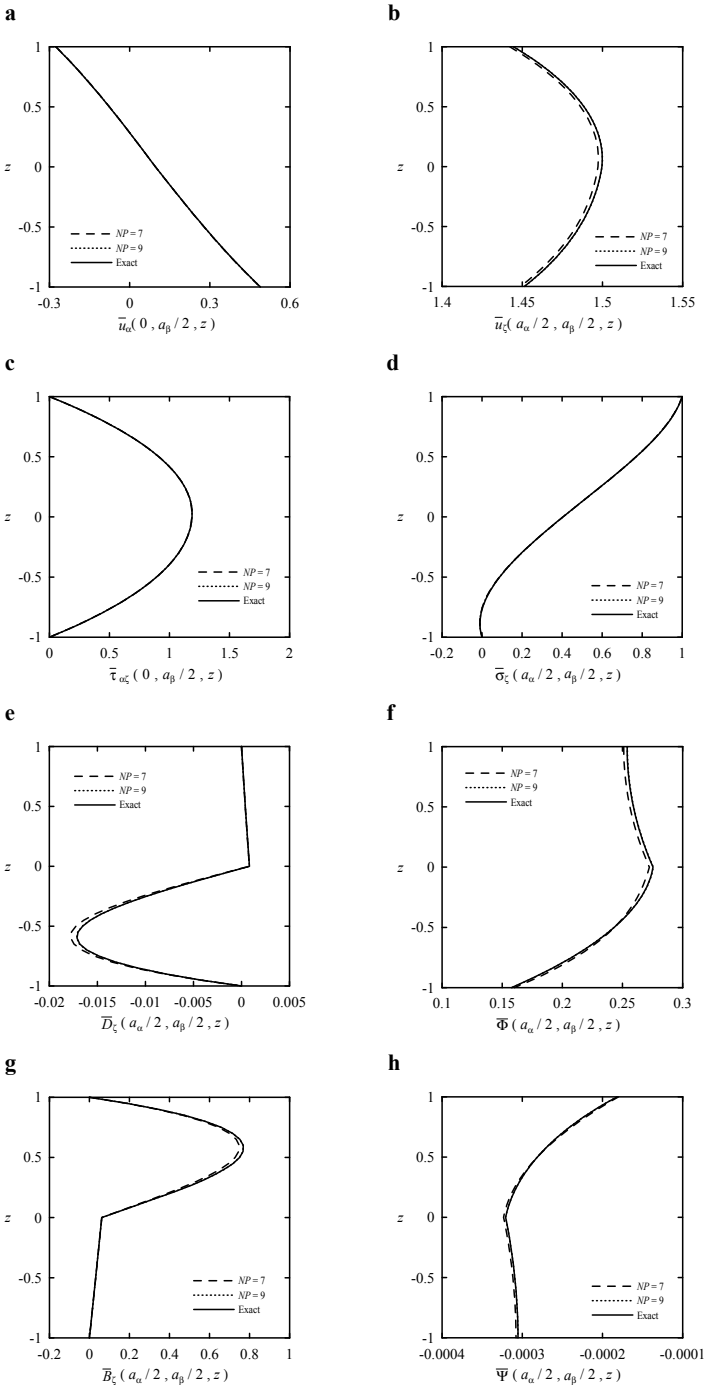

Figure 2: The through-thickness distributions of various field variables in a [F/B] shell under the mechanical load (Case 1).

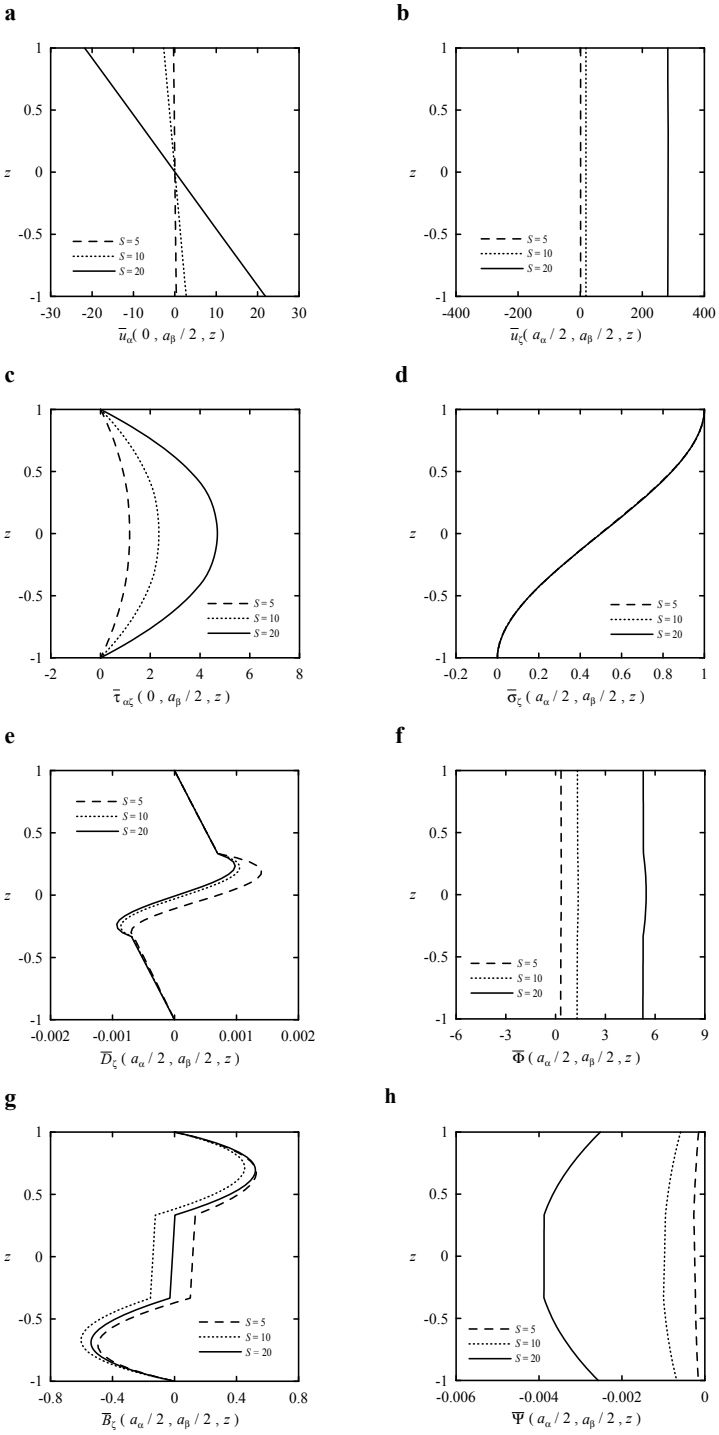

Figure 3: The through-thickness distributions of various field variables in a [F/B/F] plate under the mechanical load (Case 1).

the through-thickness distribution of the in-surface displacement appears to be linear and those of out-of-surface displacement and transverse stresses appear to be global higher-degree polynomials. It is also observed that the through-thickness distributions of variables of the electric and magnetic fields appear to be layer-wise higher-degree polynomials.

Figure 3 shows the through-thickness distributions of various variables of mechanical, electric and magnetic fields of the [F/B/F] layered shell where the span-to-thickness ratio (S) is taken to be 5, 10, 20. The other geometric parameters and dimensionless field variables are given as identical values used in the case of the [F/B] layered shell. It is shown from Fig. 3(c) that the maximum transverse shear stress occurs in the vicinity of the middle surface of the shells. The transverse shear stress produced in thick shells are smaller than that in thin shells as the shells are under mechanical loads. It is observed from Figs. 3(e)-3(f) that the electric displacement and electric potential in the thickness direction is approximately linearly varied in the magnetostrictive layer and their variations appear to be higher-degree polynomials in the electric layer. An opposite tendency is also observed for the magnetic flux and magnetic potential from Figs. 3(g)-3(h). It is shown that the magnetic potential and magnetic flux in the thickness direction is approximately linearly varied in the piezoelectric layer and their variations appear to be higher-degree polynomials in the magnetostrictive layer. The influence of span-to-thickness ratio of the shells on the electric potential and magnetic potential is much remarkable than that on electric displacement and magnetic flux.

6.3 Functionally graded magneto-electro-elastic shells

The direct and converse piezoelectric and piezomagnetic effects of doubly curved FG magneto-electro-elastic shells under the loading conditions of Cases 1-3 are considered in Figs. 4-6, respectively. The material properties of bottom and top surfaces of the shell are identical to those of $BaTiO_3$ and $CoFe_2O_4$ materials, respectively. The material properties through the thickness coordinate are assumed to obey the identical power-law distribution of the volume fractions of the constituents ($BaTiO_3$ and $CoFe_2O_4$ materials) and given as Eq. (46). The power-law exponent is taken as κ=0.1, 1, 10. The geometric parameters are considered as a_α/a_β=1, R_α/R_β=1, R_α/a_α=5 and S=$a_\alpha/2h$=10. The dimensionless variables for loading conditions of Case 1 (Eq.(34)) are given in Eq. (50). In addition, for loading conditions of Case 2 (Eq.(35)),

$$\bar{u}_i = u_i e^*/D_0(2h), \quad \bar{\tau}_{ij} = \tau_{ij} e^*/D_0 c^*, \quad \bar{\Phi} = \Phi (e^*)^2/D_0 c^* (2h), \quad \bar{D}_i = D_i/D_0,$$

$$\bar{\Psi} = \Psi q^* e^*/D_0 c^* (2h), \quad \bar{B}_i = B_i e^*/D_0 q^*. \tag{51}$$

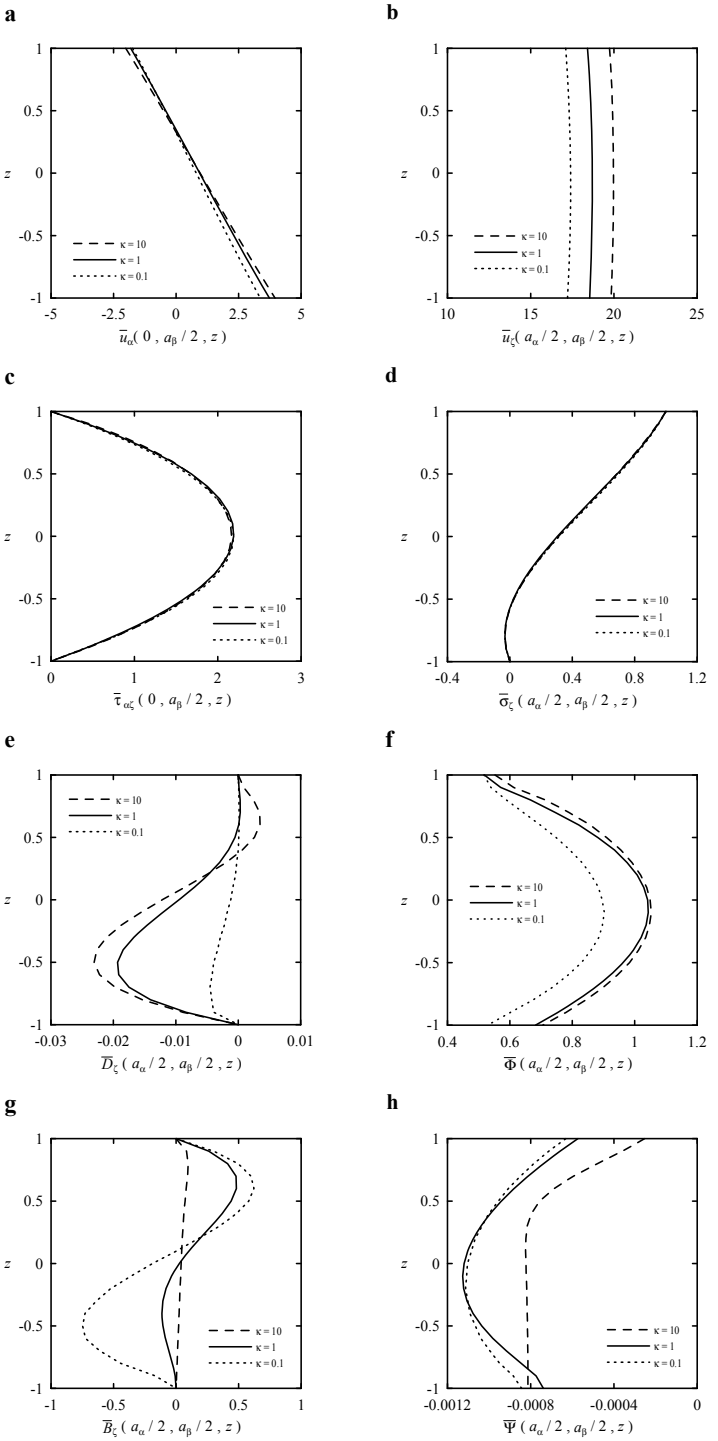

Figure 4: The through-thickness distributions of various field variables in a FG shell under the mechanical load (Case 1).

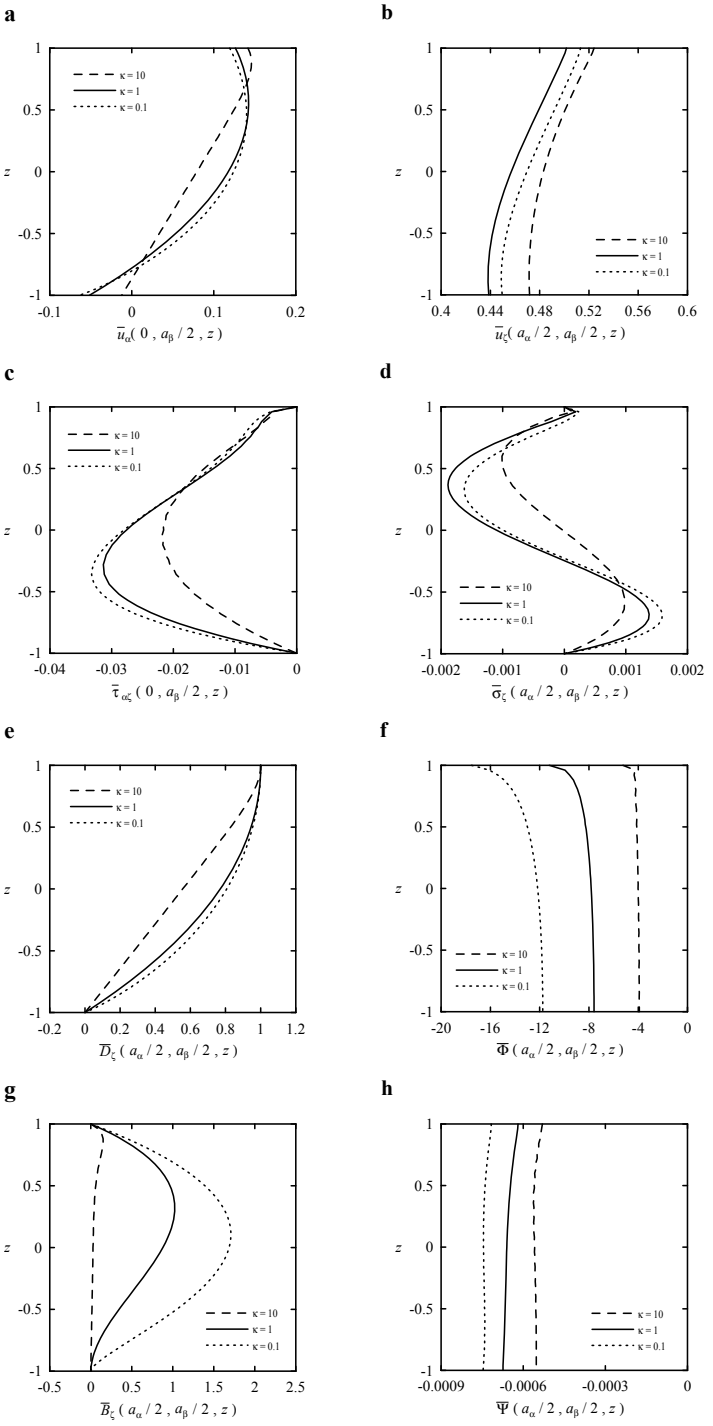

Figure 5: The through-thickness distributions of various field variables in a FG shell under the electric displacement (Case 2).

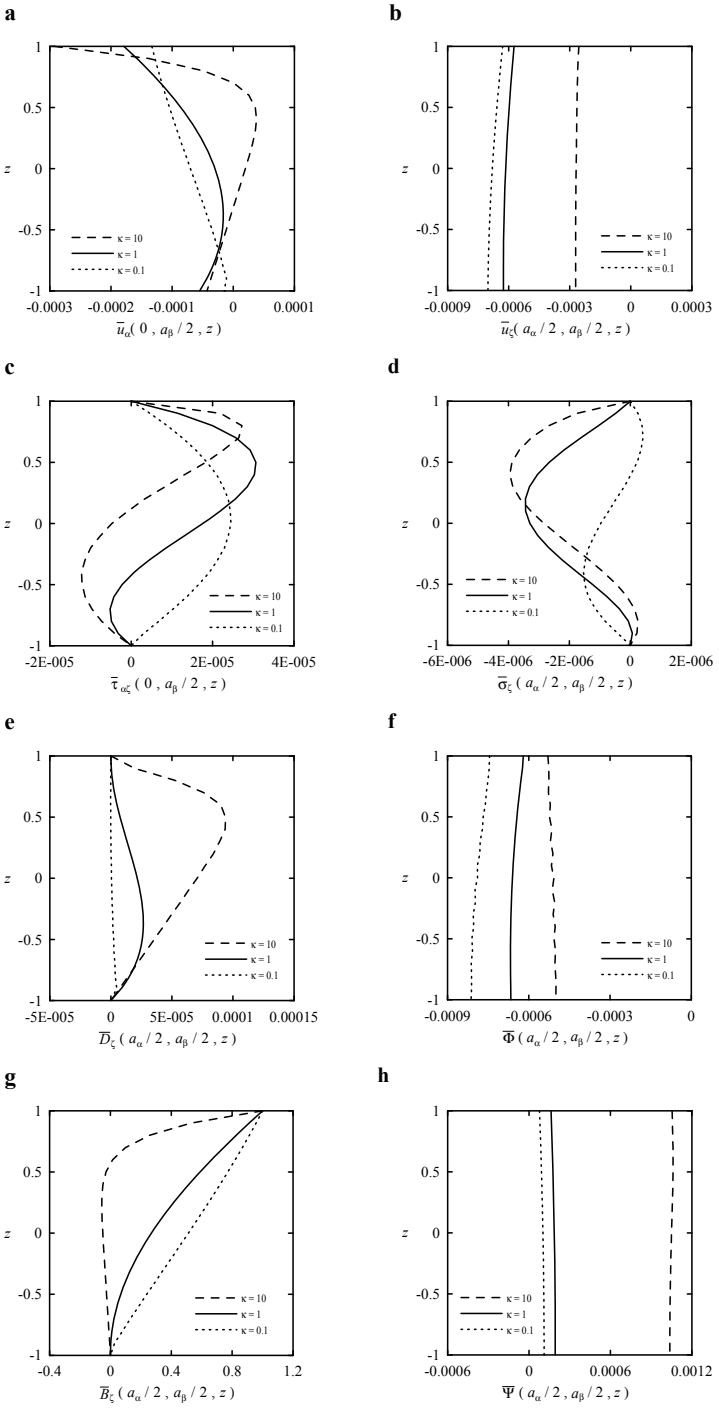

Figure 6: The through-thickness distributions of various field variables in a FG shell under the magnetic flux (Case 3).

For loading conditions of Case 3 (Eq. (36)),

$$\bar{u}_i = u_i q^* / B_0 (2h), \quad \bar{\tau}_{ij} = \tau_{ij} q^* / B_0 c^*, \quad \bar{\Phi} = \Phi e^* q^* / B_0 c^* (2h),$$

$$\bar{D}_i = D_i q^* / B_0 e^*, \quad \bar{\Psi} = \Psi (q^*)^2 / B_0 c^* (2h), \quad \bar{B}_i = B_i / B_0. \tag{52}$$

Figures 4-6 show the variations of mechanical, electric and magnetic variables across the thickness coordinate of the considered FG shells. Figures 4(a), 5(a) and 6(a) show that the through-thickness distributions of in-surface displacement appear to be linear as the mechanical load is applied; whereas that appears to be higher-degree polynomials as the electric or magnetic load is applied. It is observed from Figs. 4(a)-(d), 5(a)-(d) and 6(a)-(d) that the influence of the power-law exponent on the mechanical variables is minor in the cases of applied mechanical load (Case 1) and is significant in the cases of applied electric and magnetic loads (Cases 2 and 3). Figures 4(e)-6(e) and 4(f)-6(f) show that the electric displacement and magnetic flux change dramatically through the thickness coordinate of the shell. It is also illustrated from Figs. 4(d, e, g), 5(d, e, g) and 6(d, e, g), the prescribed boundary conditions on the lateral surfaces of the shell are exactly satisfied.

As previously observed, we found that these through-thickness distributions of generalized displacement field are quite different from the basic assumptions of kinematics field in conventionally coupled classical shell theories (CCST) and coupled first-order shear deformation theories (CFSDT), especially in the applied electric and magnetic load cases. Using CCST and CFSDT for the coupled magneto-electro-elastic analysis of FG plates and shells may lead to unexpected error. It is therefore suggested that an advanced approximate plate/shell theory needs to be developed for the coupled magneto-electro-elastic analysis of plates/shells.

7 Conclusions

In the paper we have extendedly applied the mesh-free DRK-based collocation method for the three-dimensional solutions of simply-supported, doubly curved multilayered and FG magneto-electro-elastic shells. Three different kinds of loadings (i.e., the mechanical load, electric displacement and magnetic flux) applied on the lateral surfaces of the shells are considered. The through-thickness distributions of material properties of the FG shells are considered to obey an identical power-law distribution of the volume fractions of the constituents. They are further considered as layer-wise Heaviside functions through the thickness coordinate for the analysis of multilayered shells. The accuracy and the rate of convergence of the present DRK collocation solutions are evaluated in comparison with exact solutions

of [B/F] and [F/B/F] layered magneto-electro-elastic plates available in the literature. The present asymptotic solutions are shown to converge rapidly and be in excellent agreement with the exact solutions. The variations of through-thickness distributions of magnetic, electric and mechanical variables of [F/B/F] layered shells with span-to-thickness ratios are presented. The influence of the power-law exponent on the magnetic, electric and mechanical variables induced in the FG shells is also studied. Based on the present results, it is concluded that the generalized kinematics field in CCST and CFSDT may not be appropriate for the analysis of FG and multilayered magneto-electro-elastic shells, especially as the shells are under electric and magnetic loads. Hence, an advanced approximate plate/shell theory needs to be developed for the coupled magneto-electro-elastic analysis of plates/shells. The relevant research subjects are continuously studied.

Acknowledgement: This work is supported by the National Science Council of Republic of China through Grant NSC 97-2221-E006-128-MY3.

References

Aluru, N.R. (2000): A point collocation method based on reproducing kernel approximations. *Int. J. Numer. Meth. Engng.*, vol. 47, pp. 1083-1121.

Atluri, S.N. (2004): *The Meshless Local Petrov-Galerkin (MLPG) Method for Domain & Boundary Discretizations*, Tech Science Press, 700 pages, Forsyth, GA.

Atluri, S.N.; Cho, J.Y.; Kim, H.G. (1999): Analysis of thin beams, using the meshless local Petrov-Galerkin method, with generalized moving least squares interpolations. *Comput. Mech.*, vol. 24, pp. 334-347.

Atluri, S.N.; Liu, H.T.; Han, Z.D. (2006a): Meshless local Petrov-Galerkin (MLPG) mixed collocation method for elasticity problems. *CMES: Computer Modeling in Engineering & Sceinces*, vol. 14, pp. 141-152.

Atluri, S.N.; Liu, H.T.; Han, Z.D. (2006b): Meshless local Petrov-Galerkin (MLPG) mixed finite difference method for solid mechanics. *CMES: Computer Modeling in Engineering & Sceinces*, vol. 15, pp. 1-16.

Atluri, S.N.; Zhu, T. (1998): A new meshless local Petrov-Galerkin (MLPG) approach in computational mechanics. *Comput. Mech.*, vol. 22, pp. 117-127.

Atluri, S.N.; Zhu, T. (2000a): The meshless local Petrov-Galerkin (MLPG) approach for solving problems in elasto-statics. *Comput. Mech.*, vol. 25, pp. 169-179.

Atluri, S.N.; Zhu, T. (2000b): New concepts in meshless methods. *Int. J. Numer. Meth. Engng.*, vol. 47, pp. 537-556.

Belytschko, T.; Krongauz, Y.; Organ, D.; Fleming, M.; Krysl, P. (1996): Meshless methods: An overview and recent developments. *Comput. Methods Appl. Mech. Engrg.*, vol. 139, pp. 3-47.

Belytschko, T.; Lu, Y.Y.; Gu, L. (1994): Element-Free Galerkin Methods. *Int. J. Numer. Meth. Engng.*, vol. 37, pp. 229-256.

Bhangale, R.K.; Ganesan, N. (2006): Static analysis of simply supported functionally graded and layered magneto-electro-elastic plates. *Int. J. Solids Struct.*, vol. 43, pp. 3230-3253.

Chen, J.S.; Pan, C.; Wu, C.T.; Liu, W.K. (1996): Reproducing kernel particle methods for large deformation analysis of non-linear structures. *Comput. Methods Appl. Mech. Engrg.*, vol. 139, pp. 195-227.

Chen, W.Q.; Lee, K.Y. (2003): Alternative state space formulations for magnetoelectric thermoelasticity with transverse isotropy and the application to bending analysis of nonhomogeneous plates. *Int. J. Solids Struct.*, vol. 40, pp. 5689-5705.

Han, Z.D.; Atluri, S.N. (2004a): Meshless local Petrov-Galerkin (MLPG) approaches for solving 3D problems in elasto-statics. CMES: *CMES: Computer Modeling in Engineering & Sceinces*, vol. 6, pp. 169-188.

Han, Z.D.; Atluri, S.N. (2004b): Meshless local Petrov-Galerkin (MLPG) approaches for solving 3D problems in elasto-dynamics. *CMC: Computers, Materials & Continua*, vol. 1, pp. 129-140.

Han, Z.D.; Rajendran, A.M., Atluri, S.N. (2005): Meshless local Petrov-Galerkin (MLPG) approaches for solving nonlinear problems with large deformation and rotation. CMES: *CMES: Computer Modeling in Engineering & Sceinces*, vol. 10, pp. 1-12.

Heyliger, P.R.; Ramirez, F.; Pan, E. (2004): Two-dimensional static fields in magnetoelectroelastic laminates. *J. Intell. Mater. Syst. Struct.*, vol. 15, pp. 689-709.

Heyliger, P.R.; Pan, E. (2004): Static fields in magnetoelectroelastic laminates. AIAA J., vol. 42, pp. 1435-1443.

Lancaster, P.; Salkauakas, K. (1981): Surfaces generated by moving least squares methods. *Math. Comput.*, vol. 37, pp. 141-158.

Liu, G.R.; Gu, Y.T. (2005): An Introduction to Meshfree Methods and Their Programming. Springer, 479 pages, Netherlands.

Liu, W.K.; Jun, S.; Li, S.; Adee J.; Belytschko, T. (1995): Reproducing kernel particle methods for structural dynamics. *Int. J. Numer. Meth. Engng*. vol. 38, pp. 1655-1679.

Liu, W.K.; Jun, S.; Zhang, Y.F. (1995): Reproducing kernel particle methods.

Int. J. Numer. Meth. Engng. vol. 20, pp. 1081-1106.

Lucy, L.B. (1977): A numerical approach to the testing of fission hypothesis. *Astronomical J*., vol. 82, pp. 1013-1024.

Nayroles, B.; Touzot, G.; Villon, P. (1992): Generalizing the finite element method: diffuse approximation and diffuse elements. *Comput. Mech.*, vol. 10, pp. 307-318.

Oňate, E.; Idelsohn, S.; Zienkiewicz, O.C.; Taylor, R.L. (1996): A finite point method in computational mechanics-Applications to convective transport and fluid flow. *Int. J. Numer. Meth. Engng.* vol. 39, pp. 3839-3866.

Pan, E. (2001): Exact solution for simply supported and multilayered magneto-electro-elastic plates. *J. Appl. Mech.*, vol. 68, pp. 608-618.

Pan, E.; Han, F. (2005): Exact solution for functionally graded and layered magneto-electro-elastic plates. *Int. J. Eng. Sci.*, vol. 43, pp. 321-339.

Pan, E.; Heyliger, P. (2003): Exact solutions for magneto-electro-elastic laminates in cylindrical bending. *Int. J. Solids Struct.*, vol. 40, pp. 6859-6876.

Shan, Y.Y.; Shu, C.; Lu, Z.L. (2008): Application of local MQ-DQ method to solve 3D incompressible viscous flows with curved boundary. *CMES: Computer Modeling in Engineering & Sceinces*, vol. 25, pp. 99-113.

Shu, C.; Ding, H.; Yeo, K.S. (2003): Local radial basis function-based differential quadrature method and its application to solve two-dimensional incompressible Navier-Stokes equations. *Comput. Methods Appl. Mech. Engrg.*, vol. 192, pp. 941-954.

Shu, C.; Ding, H.; Yeo, K.S. (2005): Computation of incompressible Navier-Stokes equations by local RBF-based differential quadrature method. *CMES: Computer Modeling in Engineering & Sceinces*, vol. 7, pp. 195-205.

Sladek, J.; Sladek, V.; Solek, P.; Wen, P.H. (2008): Thermal bending of Reissner-Mindlin plates by the MLPG. *CMES: Computer Modeling in Engineering & Sceinces*, vol. 28, pp. 57-76.

Sladek, J.; Sladek, V.; Solek, P.; Wen, P.H.; Atluri, S.N. (2008): Thermal analysis of Reissner-Mindlin shallow shells with FGM properties by MLPG. *CMES: Computer Modeling in Engineering & Sceinces*, vol. 30, pp. 77-97.

Sladek, J.; Sladek, V.; Zhang, C.; Tan, C.L. (2006): Meshless local Petrov-Galerkin method for linear coupled thermoelastic analysis. *CMES: Computer Modeling in Engineering & Sceinces*, vol. 16, pp. 57-68.

Sladek, J.; Sladek, V.; Wen, P.H.; Aliabadi, M.H. (2006): Meshless local Petrov-Galerkin (MLPG) method for shear deformable shells. *CMES: Computer Modeling in Engineering & Sceinces*, vol. 13, pp. 103-117.

Tsai, Y.H.; Wu, C.P. (2008a): Three-dimensional analysis of doubly curved functionally graded magneto-electro-elastic shells. *Eur. J. Mech. A/Solids*, vol. 27, pp. 75-105.

Tsai, Y.H.; Wu, C.P. (2008b): Dynamic responses of functionally graded magneto-electro-elastic shells with open-circuit surface conditions. *Int. J. Eng. Sci.*, vol. 46, pp. 843-857.

Wu, C.P.; Chiu, K.H.; Wang, Y.M. (2008a): A review on the three-dimensional analytical approaches of multilayered and functionally graded piezoelectric plates and shells. *CMC: Computers, Materials & Continua*, vol. 8, pp. 93-132.

Wu, C.P.; Chiu, K.H.; Wang, Y.M. (2008b): A differential reproducing kernel particle method for the analysis of multilayered elastic and piezoelectric plates. *CMES: Computer Modeling in Engineering & Sceinces*, vol. 27, pp. 163-186.

Wu, C.P.; Tsai, Y.H. (2007): Static behavior of functionally graded magneto-electro-elastic shells under electric displacement and magnetic flux. *Int. J. Eng. Sci.*, vol. 45, pp. 744-769.

Appendix A

The relevant coefficients in the terms of k_{ij} are given by

$$\tilde{c}_{ij} = c_{ij}/Q, \quad \tilde{e}_{ij} = e_{ij}/e, \quad \tilde{q}_{ij} = q_{ij}/q, \quad \tilde{d}_{ij} = d_{ij}Q/eq,$$

$$\tilde{\eta}_{ij} = \eta_{ij}Q/e^2, \quad \tilde{\mu}_{ij} = \mu_{ij}Q/q^2,$$

$$Q_{ij} = c_{ij} - c_{i3}a_{1j} - e_{3i}a_{2j} - q_{3i}a_{3j} \quad (i,j = 1,2,6); \quad a_{1k} = c_{k3}a_1 + e_{3k}a_2 + q_{3k}a_3,$$

$$a_{2k} = c_{k3}b_1 + e_{3k}b_2 + q_{3k}b_3, \quad a_{3k} = c_{k3}c_1 + e_{3k}c_2 + q_{3k}c_3, \quad (k = 1,2);$$

$$a_1 = \frac{1}{\Delta}\left(\eta_{33}\mu_{33} - d_{33}^2\right), \quad a_2 = \frac{1}{\Delta}\left(e_{33}\mu_{33} - d_{33}q_{33}\right), \quad a_3 = \frac{1}{\Delta}\left(q_{33}\eta_{33} - d_{33}e_{33}\right),$$

$$b_1 = a_2, \quad b_2 = \frac{-1}{\Delta}\left(c_{33}\mu_{33} + q_{33}^2\right), \quad b_3 = \frac{1}{\Delta}\left(c_{33}d_{33} + q_{33}e_{33}\right),$$

$$c_1 = a_3, \quad c_2 = b_3, \quad c_3 = \frac{-1}{\Delta}\left(c_{33}\eta_{33} + e_{33}^2\right), \quad \Delta = \begin{vmatrix} c_{33} & e_{33} & q_{33} \\ e_{33} & -\eta_{33} & -d_{33} \\ q_{33} & -d_{33} & -\mu_{33} \end{vmatrix}. \tag{A1-20}$$

Appendix B

The coefficients $\bar{k}_{ij}$ in Eq. (40) are given by

$$\bar{k}_{11} = k_{11}, \quad \bar{k}_{16} = k_{16}, \quad \bar{k}_{18} = -\tilde{m}\left(\tilde{e}_{15} h/\tilde{c}_{55}\gamma_\alpha R\right), \quad \bar{k}_{19} = -\tilde{m}\left(\tilde{q}_{15} h/\tilde{c}_{55}\gamma_\alpha R\right),$$

$$\bar{k}_{10} = -\tilde{m}\left(1/\gamma_\alpha\right), \quad \bar{k}_{22} = k_{22}, \quad \bar{k}_{27} = k_{27}, \quad \bar{k}_{28} = -\tilde{n}\left(\tilde{e}_{24} h/\tilde{c}_{44}\gamma_\beta R\right),$$

$$\bar{k}_{29} = -\tilde{n}\left(\tilde{q}_{24} h/\tilde{c}_{44}\gamma_\beta R\right), \quad \bar{k}_{20} = -n\left(1/\gamma_\beta\right), \quad \bar{k}_{33} = k_{33},$$

$$\bar{k}_{38} = -\tilde{m}^2\left[\left(\tilde{e}_{15}^2/\tilde{c}_{55} + \tilde{\eta}_{11}\right) h/\gamma_\alpha^2 R\right] - \tilde{n}^2\left[\left(\tilde{e}_{24}^2/\tilde{c}_{44} + \tilde{\eta}_{22}\right) h/\gamma_\beta^2 R\right],$$

$$\bar{k}_{39} = -\tilde{m}^2\left[\left(\tilde{e}_{15}\tilde{q}_{15}/\tilde{c}_{55} + \tilde{d}_{11}\right) h/\gamma_\alpha^2 R\right] - \tilde{n}^2\left[\left(\tilde{e}_{24}\tilde{q}_{24}/\tilde{c}_{44} + \tilde{d}_{22}\right) h/\gamma_\beta^2 R\right],$$

$$\bar{k}_{49} = -\tilde{m}^2\left[\left(\tilde{q}_{15}^2/\tilde{c}_{55} + \tilde{\mu}_{11}\right) h/\gamma_\alpha^2 R\right] - \tilde{n}^2\left[\left(\tilde{q}_{24}^2/\tilde{c}_{44} + \tilde{\mu}_{22}\right) h/\gamma_\beta^2 R\right],$$

$$\bar{k}_{51} = -\tilde{m}\left[\left(\tilde{Q}_{11}/\gamma_\alpha^2 R_x\right) + \left(\tilde{Q}_{21}/\gamma_\alpha\gamma_\beta R_y\right)\right],$$

$$\bar{k}_{52} = -\tilde{n}\left[\left(\tilde{Q}_{12}/\gamma_\alpha\gamma_\beta R_x\right) + \left(\tilde{Q}_{22}/\gamma_\beta^2 R_y\right)\right],$$

$$\bar{k}_{53} = k_{53}, \quad \bar{k}_{54} = k_{54}, \quad \bar{k}_{55} = k_{55}, \quad \bar{k}_{50} = k_{50},$$

$$\bar{k}_{61} = \tilde{m}^2\left(\tilde{Q}_{11}/\gamma_\alpha^2\right) + \tilde{n}^2\left(\tilde{Q}_{66}/\gamma_\beta^2\right), \quad \bar{k}_{62} = \tilde{m}\tilde{n}\left(\tilde{Q}_{12} + \tilde{Q}_{66}\right)/\left(\gamma_\alpha\gamma_\beta\right),$$

$$\bar{k}_{63} = -\tilde{m}\left(a_{21} e/Q\gamma_\alpha\right), \quad \bar{k}_{64} = -\tilde{m}\left(a_{31} q/Q\gamma_\alpha\right), \quad \bar{k}_{65} = -\tilde{m}\left(a_{11} h/R\gamma_\alpha\right),$$

$$\bar{k}_{66} = k_{66}, \quad \bar{k}_{60} = -\tilde{m}\left[\left(\tilde{Q}_{11}/\gamma_\alpha^2 R_x\right) + \left(\tilde{Q}_{12}/\gamma_\alpha\gamma_\beta R_y\right)\right],$$

$$\bar{k}_{71} = \tilde{m}\tilde{n}\left(\tilde{Q}_{21} + \tilde{Q}_{66}\right)/\left(\gamma_\alpha\gamma_\beta\right), \quad \bar{k}_{72} = \left[\tilde{m}^2\left(\tilde{Q}_{66}/\gamma_\alpha^2\right) + \tilde{n}^2\left(\tilde{Q}_{22}/\gamma_\beta^2\right)\right],$$

$$\bar{k}_{73} = -\tilde{n}\left(a_{22} e/Q\gamma_\beta\right),$$

$$\bar{k}_{74} = -\tilde{n}\left(a_{32} q/Q\gamma_\beta\right), \quad \bar{k}_{75} = -\tilde{n}\left(a_{12} h/R\gamma_\beta\right), \quad \bar{k}_{77} = k_{77},$$

$$\bar{k}_{70} = -\tilde{n}\left[\left(\tilde{Q}_{21}/\gamma_\alpha\gamma_\beta R_x\right) + \left(\tilde{Q}_{22}/\gamma_\beta^2 R_y\right)\right], \quad \bar{k}_{83} = k_{83}, \quad \bar{k}_{84} = k_{84}, \quad \bar{k}_{85} = k_{85},$$

$$\bar{k}_{80} = k_{80}, \quad \bar{k}_{94} = k_{94}, \quad \bar{k}_{95} = k_{95}, \quad \bar{k}_{90} = k_{90}, \quad \bar{k}_{05} = k_{05}, \quad \bar{k}_{00} = k_{00}.$$